

ELECTRONIC SUPPLEMENTARY INFORMATION

Photoisomerization of a phosphorus-based biradicaloid: Ultrafast dynamics through a conical intersection

*Tim Völzer, Henrik Beer, Axel Schulz, Stefan Lochbrunner, and Jonas Bresien**

This file includes:

1	Experimental	S2
2	Transient absorption spectroscopy	S3
3	Computational details	S11
4	References.....	S40

1 Experimental

General Information. If not stated otherwise, all manipulations were carried out under oxygen- and moisture-free conditions in an inert argon atmosphere using standard Schlenk or drybox techniques. All glassware was heated three times *in vacuo* using a heat gun and cooled under argon atmosphere. Solvents were transferred using syringes, which were purged three times with argon prior to use. Solvents and reactants were either obtained from commercial sources or synthesized as detailed in Table S1.

Table S1. Origin and purification of solvents and reactants.

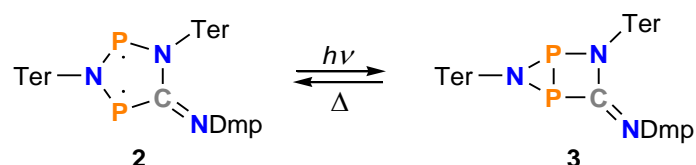
Substance	Origin	Purification
THF	local trade	dried over Na/benzophenone freshly distilled prior to use
$[\text{P}(\mu\text{-N}^{\text{Ter}})]_2\text{DmpNC}$	synthesized ^[1]	Re-crystallized as described in the literature ^[1]

UV-Vis spectra were acquired on a Perkin-Elmer Lambda 19 UV-Vis spectrometer.

The setup for **transient absorption spectroscopy** is described in section 2.2.

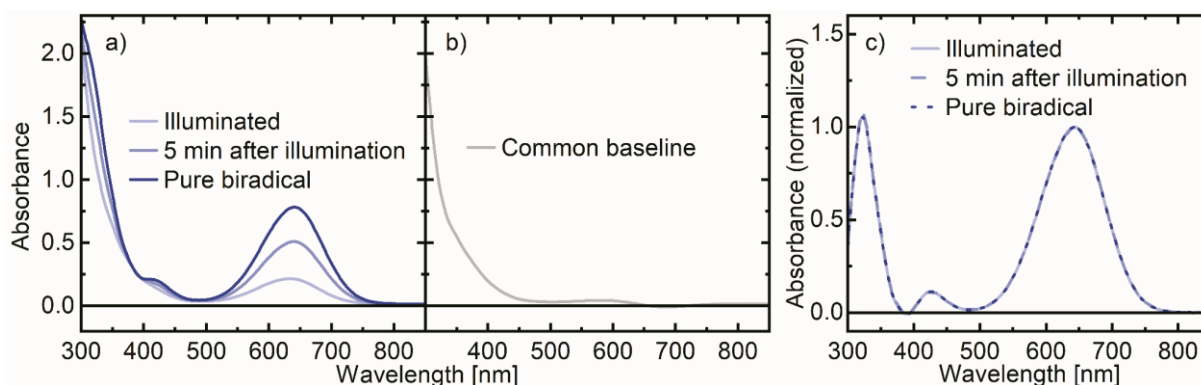
2 Transient absorption spectroscopy

2.1 Static absorption of biradical (2) and housane (3) species



To gain an overview of possible or expected signatures in the transient spectra, we first compared the static absorption of the (ground state) biradical (**2**) vs. the housane isomer (**3**). To this end, we measured the absorption spectra of a solution of **2** in THF (ca. 1.2 mg/3 mL THF) in its original state as well as immediately and 5 min after illumination (flash light) which triggered the conversion of the biradical into the housane species **3**. Figure S1a contains the respective absorbance spectra referenced to a cuvette with pure solvent. As can be seen from the curves, the absorption strictly rises with an increasing fraction of the biradical isomer in the solution.

Figure S1. Decomposition of the static absorption of mixtures of biradical (**2**) and housane (**3**) into common and difference absorption of **2** and **3**. a) Absorption spectra of a solution of **2** prior to and after illumination with a flashlight. b) Baseline absorption $A_0(\lambda)$ common to all three spectra in Figure S1a with strong absorption in the UV due to the organic substituents. c) Normalized difference absorption $A_\Delta(\lambda)$ for the three curves in Figure S1a. All lines are virtually identical.



Since the overall number of solute molecules remains constant during structural conversion, we may express the measured spectra as a linear combination of some

constant baseline absorption $A_0(\lambda)$ (common to both of the species and thus probably originating from the organic substituents) and the difference spectrum $A_\Delta(\lambda)$ between **2** and **3** scaled with the proportion of the former in the mixture.

$$A_i(\lambda) = A_0(\lambda) + \alpha_i \cdot A_\Delta(\lambda) \quad (\text{S1})$$

Based on this representation, we extracted the baseline absorption as depicted in Figure S1b, showing strong absorption only in the UV region. The difference spectra, obtained by subtracting $A_0(\lambda)$ from the original data, are normalized and compared in Figure S1c. All three curves are practically identical and non-negative throughout the entire spectral regime. Hence, we conclude that neither **3** exhibits any additional absorption with reference to **2** nor does its presence shift or broaden any absorption bands. Consequently, we expect only bleach signals in the transient absorption (TA) spectra due to the photoinduced conversion from (ground state) biradical to (ground state) housane species. Accordingly, any increased absorption signal, shifts or broadenings must be associated with electronically excited or other intermediate states.

2.2 Pump-probe setup with a sample flow system

The TA measurements were performed with a pump-probe setup similar to the one described by Megerle *et al.*^[2] Starting from the output of a regenerative Ti:sapphire-amplifier (Spitfire Ace, 1kHz @ 800 nm), pump pulses with a centre wavelength of 650 nm and a duration of 29 fs (FWHM) were generated by a noncollinear optical parametric amplifier. Parallel, a small fraction of the fundamental beam was used to create a white light supercontinuum for probing by self-phase modulation in a calcium fluoride substrate. This beam was again split into two parts. One was focussed onto the sample, while the other one was detected separately to track and correct (spectral) fluctuations in the white light continuum. At the sample position, the probe spot exhibited a $1/e^2$ -diameter of 60 μm , while the pump spot extended to 150 μm ,

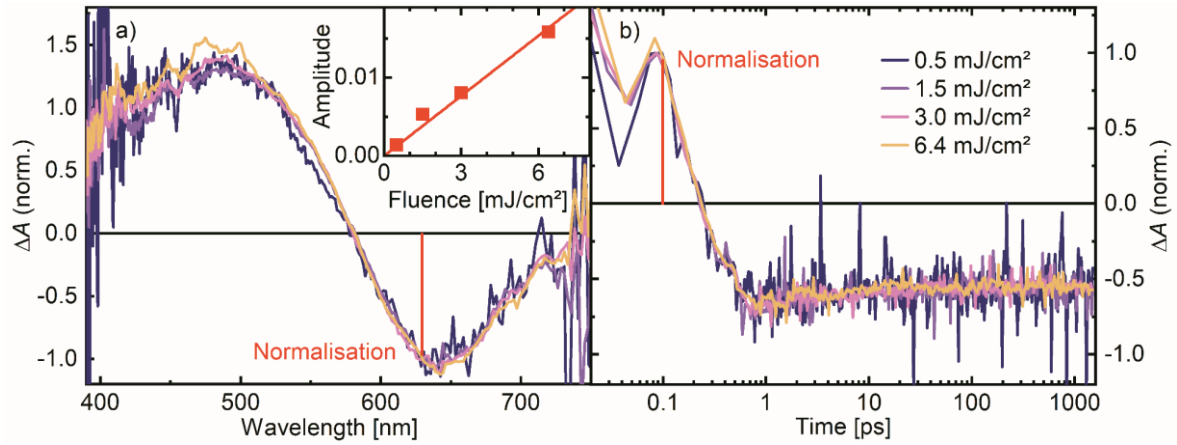
containing a maximum pulse energy of 700 nJ. This corresponds to a maximum excitation fluence of about 7 mJ cm^{-2} , which could also be tuned using a pair of polarisers. Additionally, the polarisation of the pump relative to the probe beam was adjusted via a half-wave plate in the former.

To avoid contributions from photobleaching of **2**, which would result in a fast extinction of the absorption and thereby likewise of the TA signal during measurements, the sample solution had to be in a steady flow to provide non-bleached sample for each consecutive laser shot. Additionally, as oxygen and water contamination leads to the degradation of the molecules, the solution had to be investigated under the exclusion of ambient air. To meet these requirements, the TA measurements were performed in a pumped flow cell system (Starna UTWA/2 cuvette with $100 \mu\text{m}$ thickness, Micropump GA-t23.jfsb with DB380B motor), with the pump cycle being filled and sealed under argon atmosphere in a glove box.

2.3 Excitation fluence dependence of the transient signals

In this section, we examine the behaviour of the transients under the influence of an altered excitation density to exclude any nonlinear effects that could possibly affect the spectral shape or the dynamics, especially concerning the quality of the fits. To that end, we tuned the pump pulse energy stepwise from 50 to 650 nJ and measured the evolution of the transient spectra, respectively. The spectra at a probe delay of 65 fs, normalised to the negative amplitude at 630 nm, as shown in Figure S2a, appear fairly similar. On top of that, the inset proves an approximately linear growth of the amplitude with rising fluence, excluding a significant effect of nonlinear features such as saturated or two-photon absorption. Likewise, the time traces in Figure S2b exhibit identical shapes, suggesting the absence of any nonlinear dynamics. This proves the analysis conducted for measurements at 3 mJ cm^{-2} to represent the entire examined fluence regime.

Figure S2. Fluence dependence of the transient signals. a) Normalised transient spectra for a probe delay of 65 fs with various pump fluences. Within their noise level, all curves are almost identical. The vertical, red line indicates the wavelength considered for normalisation. The respective absolute amplitudes are depicted in the inset with a corresponding linear fit (red line). b) Normalised time traces at 562 nm for different excitation fluences. The deviations between the four curves are below the noise-related measurement uncertainty. The vertical, red line marks the probe delay at which normalisation was carried out.



2.4 Anisotropy dynamics

Generally, linearly polarised pump light induces an excitation anisotropy, resulting in differences between the TA signals obtained with parallel and perpendicular probe light in polarisation-resolved measurements.^[3] The differences decay as the excited molecules thermally turn into a random orientation distribution, obliterating the anisotropy. In the magic angle configuration, however, the anisotropy from parallel and perpendicular orientation cancel out. Accordingly, the corresponding transient signal in the magic angle case can be calculated from the parallel and the perpendicular case as follows:

$$\Delta A_{\text{mag}}(\lambda, t) = \frac{\Delta A_{\parallel}(\lambda, t) + 2 \cdot \Delta A_{\perp}(\lambda, t)}{3} \quad (\text{S2})$$

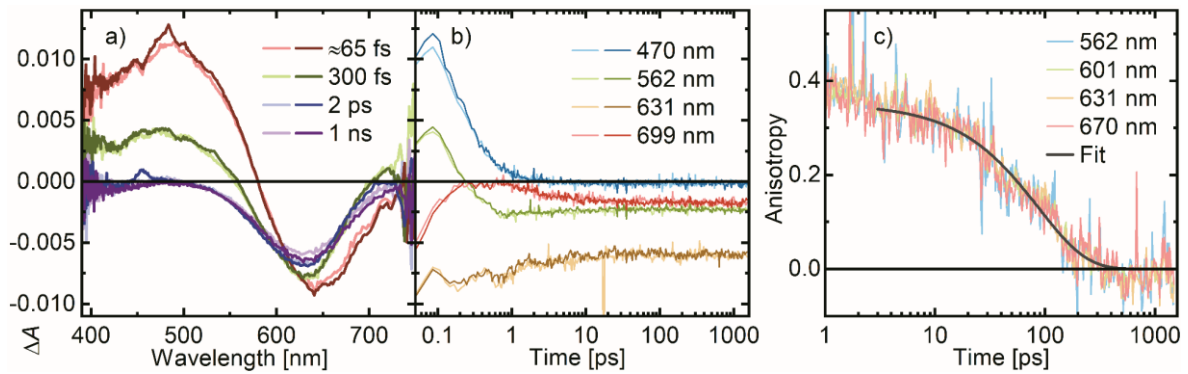
with ΔA_{mag} , ΔA_{\parallel} , and ΔA_{\perp} denoting the transient signal in magic angle, parallel and perpendicular configuration, respectively. In Figure S3a and b, we compare the magic angle data to this weighted average of the signals with parallel and perpendicular

orientation in both wavelength and time domain, finding an excellent agreement of the respective curves. This confirms the correct orientation of the polarisations in all three cases. On that basis, we may now investigate the TA anisotropy a defined as

$$a(\lambda, t) = \frac{\Delta A_{\parallel}(\lambda, t) - \Delta A_{\perp}(\lambda, t)}{\Delta A_{\parallel}(\lambda, t) + 2 \cdot \Delta A_{\perp}(\lambda, t)} \quad (\text{S3})$$

The temporal evolution of the anisotropy at various wavelengths in the spectral region of the ground state bleach is depicted in Figure S3c, with identical progressions for all curves. Their decay is accurately fitted with a monoexponential function, yielding an anisotropy lifetime of $\tau_{\text{aniso.}} \approx 90$ ps.

Figure S3. Polarisation check and anisotropy decay. a) Transient spectra and b) time traces in magic angle configuration for various probe delays and wavelengths, respectively. The pale colours mark the data measured with the corresponding polarisation orientation, while the dark ones represent the weighted average of parallel and perpendicular polarisation as given in equation (S2). c) Anisotropy as calculated from equation (S3) for several wavelengths in the bleach regime. The black line illustrates the result of a single-exponential fit.

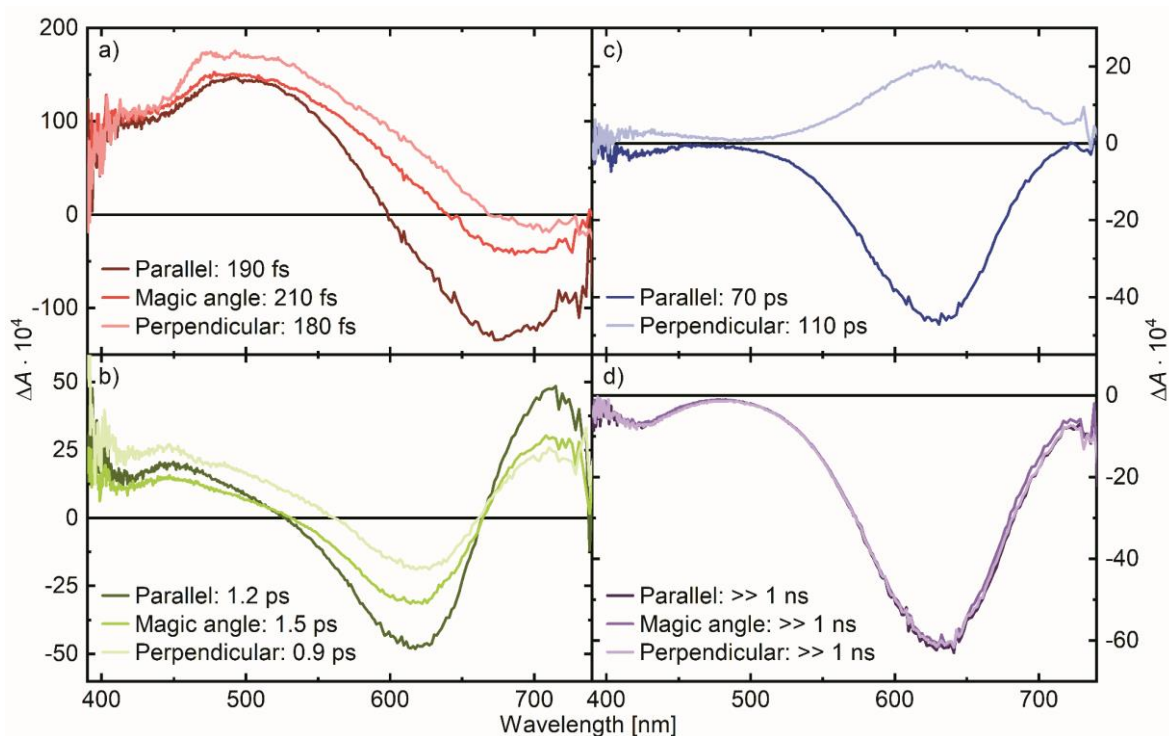


2.5 Polarisation-resolved amplitude spectra

In the following, we investigated the polarisation dependence and anisotropy of the transient signals. To that end, we globally fitted the TA measured in parallel, magic angle and perpendicular configuration. Note that in the parallel and perpendicular case, we implemented an additional fourth exponential component to account for the anisotropy dynamics, which, in turn, cancel out when probing with magic angle

polarisation. Figure S4 illustrates the amplitude spectra for each separate process of the ultrafast dynamics while systematically comparing the different polarisations and indicating the individual time constants.

Figure S4. Amplitude spectra and corresponding time constants in dependence on the relative polarisation of pump vs. probe. Perpendicular, magic angle and parallel polarisation are indicated by increasingly dark colours, respectively. a) Relaxation through conical intersection. At long wavelengths, the signal strongly depends on the polarisation, while the short-wavelength region lacks any systematic dependence. b) Geometrical rearrangement. The spectral polarisation dependence bears strong similarities with Figure S4a. c) Anisotropy decay. This feature does not appear in the magic angle configuration due to cancelling of all polarisation effects. The contributions from parallel and perpendicular polarisation are opposite in sign with an amplitude ratio of 2. d) Quasi-constant long-term bleach resulting from slow reversion to the biradical form (**2**). The curves are identical for all polarisations.



2.5.1 Electronic relaxation through conical intersection

For the fastest component (Figure S4a), the polarisation dependence changes throughout the visible spectrum. While the ESA feature in the blue spectral region is essentially not altered by turning the probe relative to the pump polarisation, the GSB is enhanced for parallel and suppressed for perpendicular orientation. We explain the

latter by the selective absorption of light whose linear polarisation lies preferably parallel to the transition dipole moment. Consequently, the dipole moment for the ESA, in contrast, is strongly tilted with respect to that of the ground state. On top of the different polarisation dependences, we note a strong overlap of GSB and ESA. As the former shrinks at perpendicular probing, we observe the expanse of the positive signal into the red spectral region. Considering that the GSB amplitude ought to triple from perpendicular to parallel configuration, we expect the polarisation-independent ESA to cover the entire visible range. Hence, both spectral signal as well as the dynamics of both contributions partially compensate. This accounts for the discrepancy between the calculated maximum GSB amplitude of $\Delta A = -0.024$ for the magic angle configuration and the maximum measured negative signal of $\Delta A = -0.008$. Likewise, this explains why (despite three quarters of the excited **2** population relaxing through the conical intersection back into their electronic ground state) the transient signal in the GSB spectral region undergoes merely small changes during this first dynamics.

2.5.2 Geometrical rearrangement in the electronic ground state

Considering the amplitude spectra for the structural realignment of the biradical molecules, as depicted in Figure S4b, we observe a polarisation dependence similar to the one for the fastest component. The positive, short-wavelength contribution exhibits no systematic variation with probe orientation while the positive and negative peaks at longer wavelengths experience a rise in amplitude from perpendicular to parallel configuration. Accordingly, the latter two are associated with changes in the GSB. Note that the discrepancy between the obtained time constants may result as artefacts from the superposing anisotropy dynamics in the case of parallel and perpendicular probing.

2.5.3 Spectral anisotropy dynamics and long-term equilibrium

After the rearrangements of the geometrical structure, the only difference to the original state prior to pumping is the roughly 25% of the excited molecules remaining in the hausane form. As they lack any additional absorption feature, the transient signal

consists solely of the bleach corresponding to the missing biradical absorption. Yet, the anisotropy persists, thus resulting in a stronger bleach signal for probing parallel to the pump polarisation. Consequently, as the anisotropy decays, the bleach amplitude shrinks in the parallel case and grows for a perpendicularly oriented probe. Accordingly, we observe a negative and a (except for a factor of one half) identical positive amplitude spectrum in Figure S4c, respectively. Furthermore, the time constants obtained for these signatures are consistent with the one extracted from the anisotropy fit discussed in section 2.4. All in all, we attribute these features to the decaying excitation anisotropy.

In the aftermath of this orientation relaxation, the remaining transient bleach signal behaves isotropic regarding the probe polarisation. The identical amplitude spectra in Figure S4d, describing the long-term temporal evolution of the transient spectra, prove the absence of any residual polarisation dependence. Due to the extremely slow reconversion from hausane to biradical species with a half-life in the range of 7 min, well beyond the examined time span of about 1.5 ns, we do not observe further dynamics, as expressed by the essentially infinite time constants yielded by the fit.

3 Computational details

3.1 General remarks

Computations were carried out using Gaussian 09^[4] and ORCA 4.2.1.^[5]

Density functional theory (DFT) calculations employed either the pure exchange-correlation functional PBE^[6,7] or the corresponding hybrid functional PBE0^[6-8] in conjunction with Grimme's dispersion correction D3(BJ)^[9,10] and the def2-TZVP basis set^[11] (notation PBE-D3/def2-TZVP or PBE0-D3/def2-TZVP). The resolution of identity (RI) approximation was applied for the pure density functional PBE, using Weigend's Coulomb fitting basis.^[12] The stability of the all Kohn-Sham wavefunctions was analysed, and the unrestricted "broken symmetry" solution was used where appropriate.

Ab-initio calculations employed the Complete Active Space SCF (CASSCF) method,^[13-21] which correctly describes the multireference character of the investigated systems (i.e. treatment of non-dynamic correlation). To account for dynamic correlation, the CASSCF reference wavefunctions were employed in multireference perturbation calculations, using the Strongly Contracted *N*-Electron Valence State Perturbation Theory (SC-NEVPT2).^[22-24] Alternatively, the CASSCF reference was employed in multireference configuration interaction (MRCI) calculations with single and double substitutions. The perturbative multi-reference Davidson correction for disconnected quadruple substitutions was applied (i.e. MRCISD+Q).^[25,26] For further information on the MRCISD computations, please also refer to the SI of our previous publication.^[27]

Structure optimizations were performed using analytic gradients. The optimized structures were confirmed as minima or transition states using either analytic or numeric frequencies. Please note that all computations were carried out for single, isolated molecules in the gas phase (ideal gas approximation).

3.2 Study of the PES using a model system

The model system **2H** (i.e. all substituents replaced by H) was used to study the potential energy surface (PES) of the ground state (S_0) and first excited singlet state (S_1) in detail.

On the ground state PES, minima for biradical **2H** and housane **3H** were located at the PBE-D3/def2-TZVP level of theory. Furthermore, the transition state (TS), which describes the thermal reverse reaction **3H** \rightarrow **2H**, was optimized at the UPBE-D3/def2-TZVP level of theory. An intrinsic reaction coordinate (IRC) scan^[28,29] was performed to confirm that the TS connects the correct minima on the PES (Figure S5).

The TS structure was then further optimized at the CAS(2,2)/def2-TZVP level of theory, using a correct multireference description of the wavefunction. Starting from this optimized TS structure, an IRC scan was performed at the same level of theory, resulting in a minimum energy path that connects both minima **2H** and **3H**. To account for dynamic correlation and to obtain a vertical excitation profile along the reaction path (see below), single-point state-averaged NEVPT2/CAS(2,2)/def2-TZVP calculations were performed for every point of the IRC scan (Figure S5 and Figure S6).

Figure S5. Ground state minimum energy path (MEP) between biradical **2H** and housane **3H**. The DFT and NEVPT2/CASSCF results are in reasonable agreement (see also Table S2).

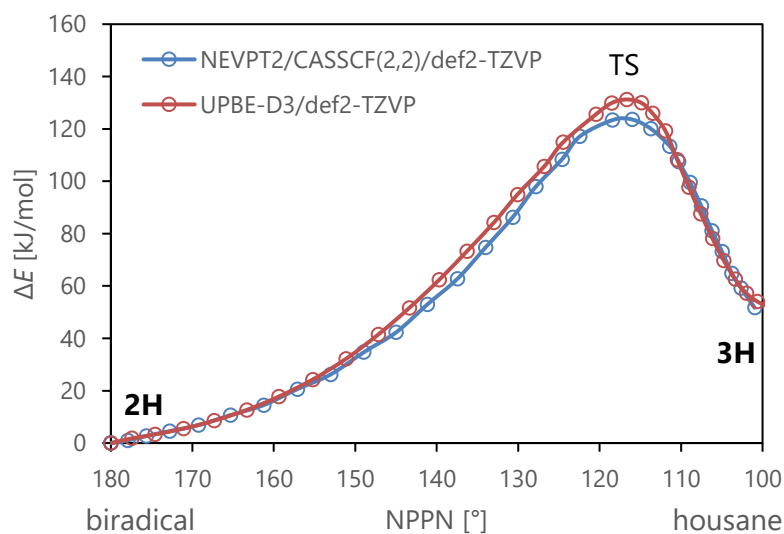
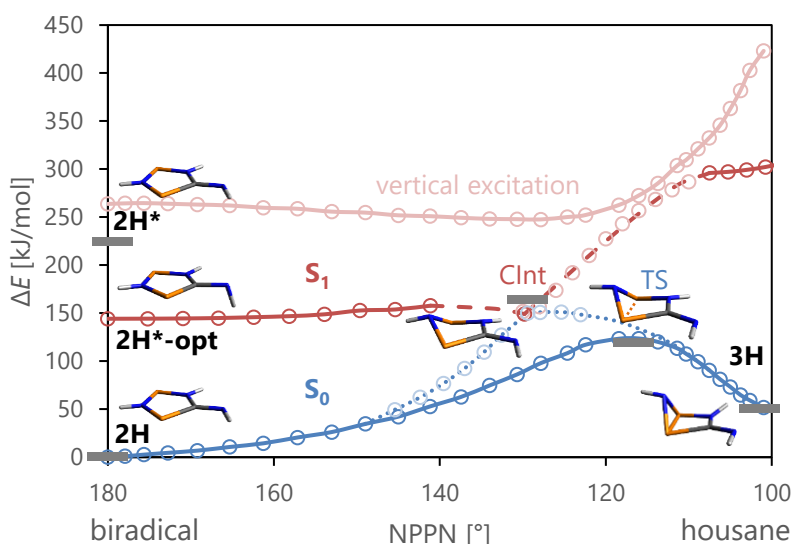


Table S2. Relative electronic energies (E_{tot} in kJ/mol) of the stationary points of the PES.

	DFT ^[a]	NEVPT2/CAS(2,2) ^[b]	MRCI+Q/CAS(8,6) ^[c]
2H (S_0)	0.0	0.0	0.0 ^[27]
2H* (S_1) ^[d]	249.0	263.9	224.9 ^[27]
3H (S_0)	43.8	42.3	50.4 ^[27]
TS (S_0)	131.9	124.4	119.4
Clnt	149.0	162.6	163.7 ^[e]
2H (T_1) ^[d]	106.5	98.4	76.9

[a] UPBE-D3/def2-TZVP; [b] NEVPT2/CAS(2,2)/def2-TZVP energies, geometries optimized at CAS(2,2)/def2-TZVP; [c] MRCISD+Q/CAS(8,6)/def2-TZVP energies, geometries optimized at UPBE-D3/def2-TZVP; [d] vertical excitation energy; [e] geometry optimized at state-averaged CAS(8,6)/def2-TZVP,^[27] average between S_0 and S_1 is reported.

Figure S6. Ground state (S_0) and first excited singlet state (S_1) surfaces projected along the NPPN dihedral angle. The blue and red lines correspond to the minimum energy paths (MEPs) of the S_0 (state-averaged NEVPT2/CAS(2,2)/def2-TZVP, cf. Figure S5) and S_1 state (TD-DFT/TDA PBE-D3/def2-TZVP, energies with respect to S_0 PES in Figure S5), respectively. The faded red line indicates the vertical excitation profile (state-averaged NEVPT2/ CAS(2,2)/def2-TZVP), i.e. the first excited state energy at the respective ground state geometry. Note that this is a very simplified picture which projects multidimensional hyperlines into a 1D diagram, i.e. the different lines should be pictured in different "layers" of the diagram. The results of MRCI+Q/CAS(8,6)/def2-TZVP computations^[27] are indicated as grey bars.



Further studies of the excited state PES were performed using the TD-DFT method^[30-32] and Tamm-Dancoff-Approximation (TDA), as state-specific CASSCF computations

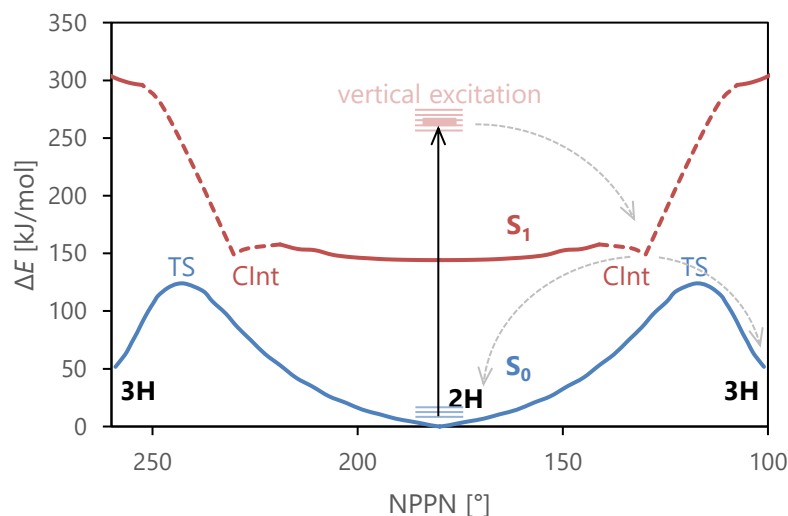
(which would be required for optimization of excited state structures using the CASSCF method) failed due to problems with root flipping.

Geometry optimization of the S_1 state located a shallow minimum (**2H*-opt**) close to the vertically excited structure **2H*** (Figure S6), which comprises a planar five-membered ring system. However, the exocyclic C–N group is twisted by approx. 90° compared to the ground state geometry (Figure S6). A completely planar structure resembling the ground state structure corresponds to a transition state on the S_1 PES, which describes the rotation of the C–N bond (see also Figure S9). The rotational barrier is $\Delta E_{\text{tot}} = 57.4$ kJ/mol or $\Delta G^\ddagger = 29.1$ kJ/mol. Note that both stationary points lie energetically well below the vertically excited structure **2H*** (ΔE_{tot} to TS: -46.7 kJ/mol, **2H*-opt**: -104.1 kJ/mol), i.e. the vertically excited molecules are in a highly excited vibrational state within the electronic S_1 surface, so that the low rotational barrier for C–N bond rotation is effectively irrelevant.

Next, a relaxed surface scan along the NPPN dihedral was performed, which corresponds to the reaction coordinate that leads to a conical intersection (CI_{nt}) with the electronic ground state. The NPPN dihedral, which describes the folding of the ring system along the P–P axis, is an orthogonal coordinate to the C–N bond rotation. The scan revealed that the folding potential is very flat and leads to the CI_{nt} in an almost barrier-free process (Figure S6).

A similar scan was performed starting from vertical excitation of the housane **3H**. Here, no minimum is found on the S_1 PES. Instead, the MEP leads directly to the CI_{nt} (Figure S6). Note that the potential on this side of the CI_{nt} is rather steep and forms the side of the potential well which formally describes the boundary of the vibrational states of the vertically excited biradical **2H** (Figure S7). Thus, in a simplified picture, the vertically excited molecules of **2H** can reach the CI_{nt} solely by vibrational relaxation, which is expected to be quite fast.

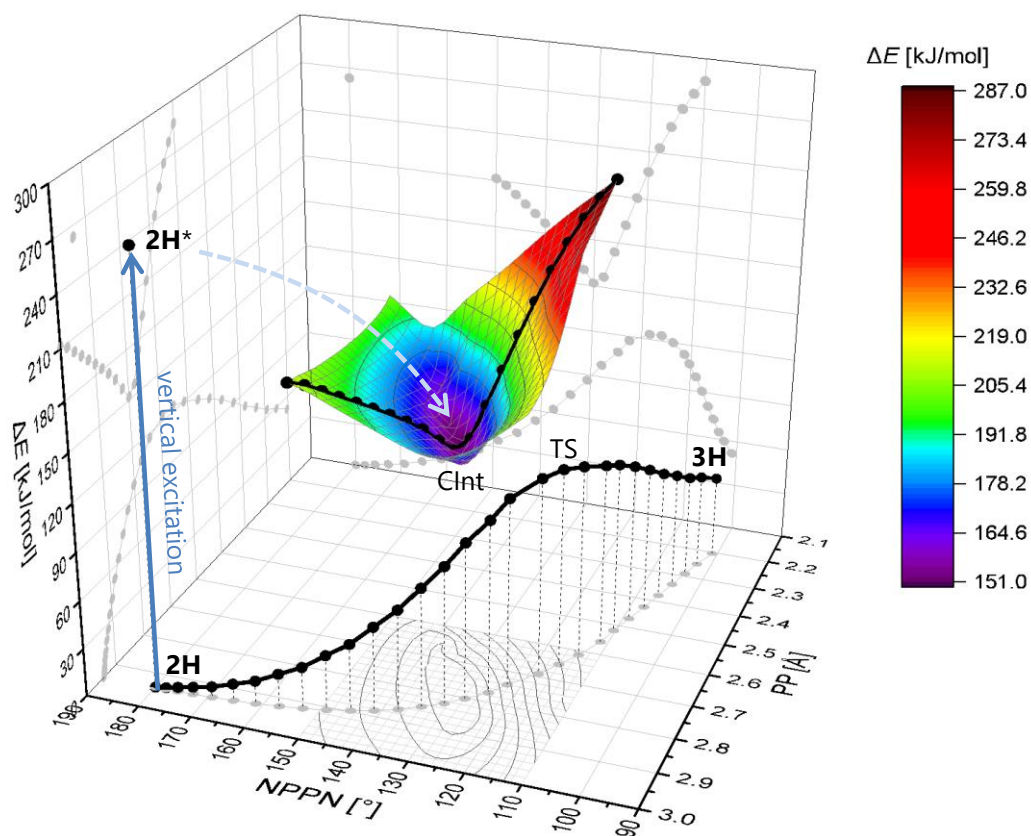
Figure S7. Ground state (S_0) and first excited singlet state (S_1) MEPs projected along the NPPN dihedral angle. Vibrational levels are schematically indicated by thin horizontal lines (not to scale).



The Clnt was optimized at the TD-DFT/TDA PBE-D3/def2-TZVP level of theory using the algorithm implemented in ORCA,^[5] as well as by the aid of state-averaged CAS(2,2) and CAS(8,6)^[27] computations using Gaussian 09. The results of the different approaches agree reasonably well (Table S2 and Figure S6). The energy difference between S_1 and S_0 PES vanishes at this point ($\Delta E < 0.1 \text{ mE}_h$).

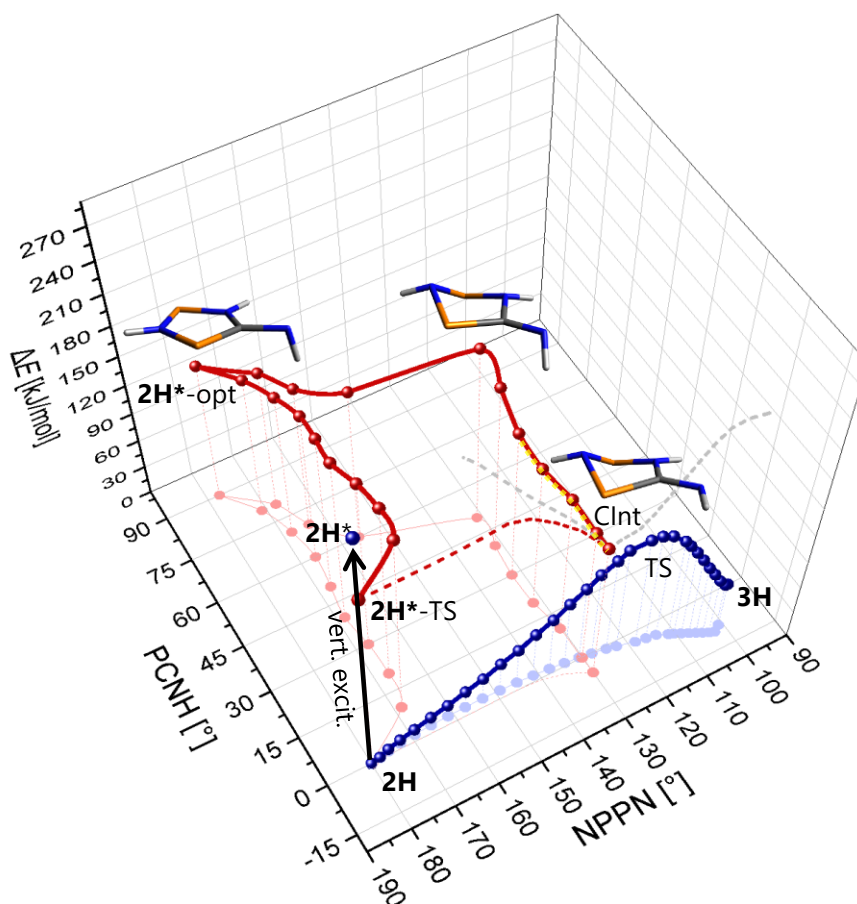
To obtain an idea of the shape of the cone around the Clnt, a 2-dimensional relaxed surface scan along the NPPN dihedral angle as well as the P–P interatomic distance was performed using the Clnt optimizer and the TD-DFT/TDA method. The resulting excited state PES describes the region where the energy difference between the S_1 and S_0 electronic states is minimized, and it vanishes at the minimum of the cone (Figure S8). It is worthy to note that the Clnt is located near the TS of the ground state reaction path, however on the biradical side along the MEP, in agreement with the experimentally observed quantum yield of the switching process of ca. 25% (i.e. 75% of the excited molecules revert back to the biradical **2**).^[27] Moreover, the gradient towards the biradical **2H** is much steeper than the gradient towards the housane **3H** (Figure S6), so the observed product distribution is plausible.

Figure S8. 3-dimensional plot of the relative energy ΔE (in kJ/mol) versus NPPN dihedral and PP distance. The ground-state MEP (NEVPT2/CAS(2,2)/def2-TZVP) is shown as solid black line connecting the biradical (**2H**) and housane (**3H**) via a single transition state (TS); the steps of the IRC scan are indicated as black dots. The 2D surface around the conical intersection (Clnt) represents a relaxed PES of the S_1 state that minimizes the energy difference between S_1 and S_0 state (TD-DFT/TDA PBE-D3/def2-TZVP). The black line that intersects the surface is approximately parallel to the ground state reaction coordinate and roughly corresponds to the gradient difference vector^[33,34] of the Clnt.



On a last note, it should be mentioned that the S_1 MEP shown in Figure S6 is “discontinuous” in the region of the Clnt, i.e. structure optimization failed in this region unless an additional degree of freedom was removed by projecting the gradient difference between both states out of the mean energy gradient (as is done by the Clnt optimization procedure). Thus, the “normal” relaxed surface scan starting from the excited biradical or housane structure was aborted in the vicinity of the Clnt, and instead the surface of the Clnt was scanned as described above. This may lead to small “jumps” in other coordinates that are not displayed; however, this should not affect the general picture.

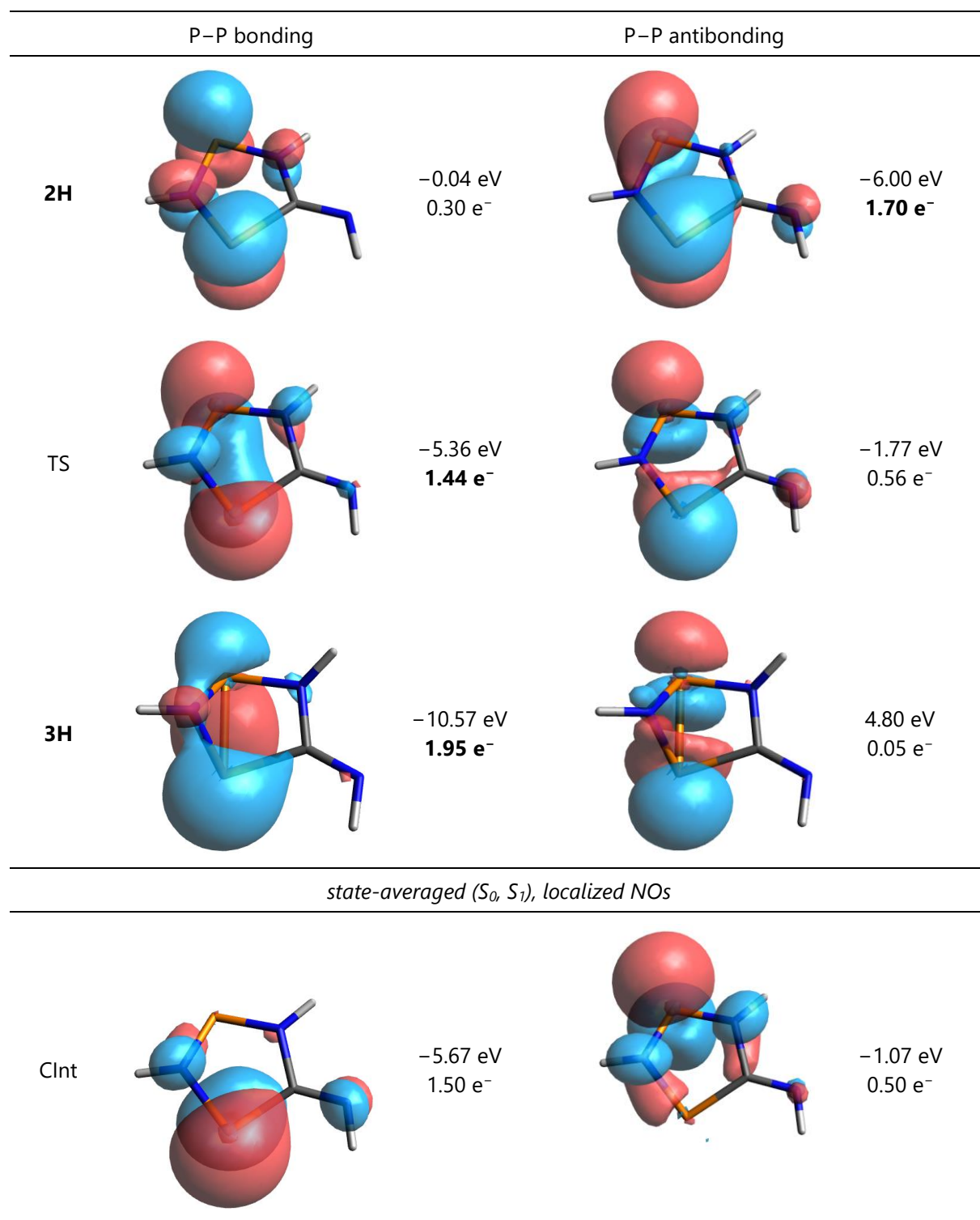
Figure S9. PES projected along the PCNH and NPPN dihedral angles. The ground state MEP (blue) is nearly independent of the PCNH dihedral. The solid red line indicates the approximate MEP on the S_1 PES (the line connecting **2H*-opt** and the Clnt corresponds to the S_1 MEP in Figure S6). In the region of the extended conical intersection seam^[35] (dashed orange line), the S_0 and S_1 states are degenerate; the Clnt is the minimum on this hyperline which is perpendicular to the NPPN dihedral angle. The cone of the Clnt (grey) is projected along the same coordinate as in Figure S8. The shortest path from the TS to the Clnt (dashed red line) indicates that the S_1 PES is rather flat in this region.



Using the Clnt optimization algorithm, a continuous path between **2H*-opt** and the Clnt was found when scanning along the PCNH dihedral angle, which describes rotation of the C–N bond (Figure S9). (Note that this path is not necessarily the MEP, as the energy difference between S_1 and S_0 is optimized as well in this procedure.) As explained above, this coordinate is orthogonal to the ground state MEP; thus the overall photochemical and thermal process cannot be fully described by a single coordinate. The energy barrier along this path is approx. $\Delta E_{\text{tot}} = 38$ kJ/mol and thus comparable to the rotational barrier discussed above. (Note that this barrier is an upper

bound for the true energy barrier along the MEP.) Due to the large energy excess of the vertically excited molecules, this low barrier is not expected to play a significant role in the deactivation of the system through the Clnt.

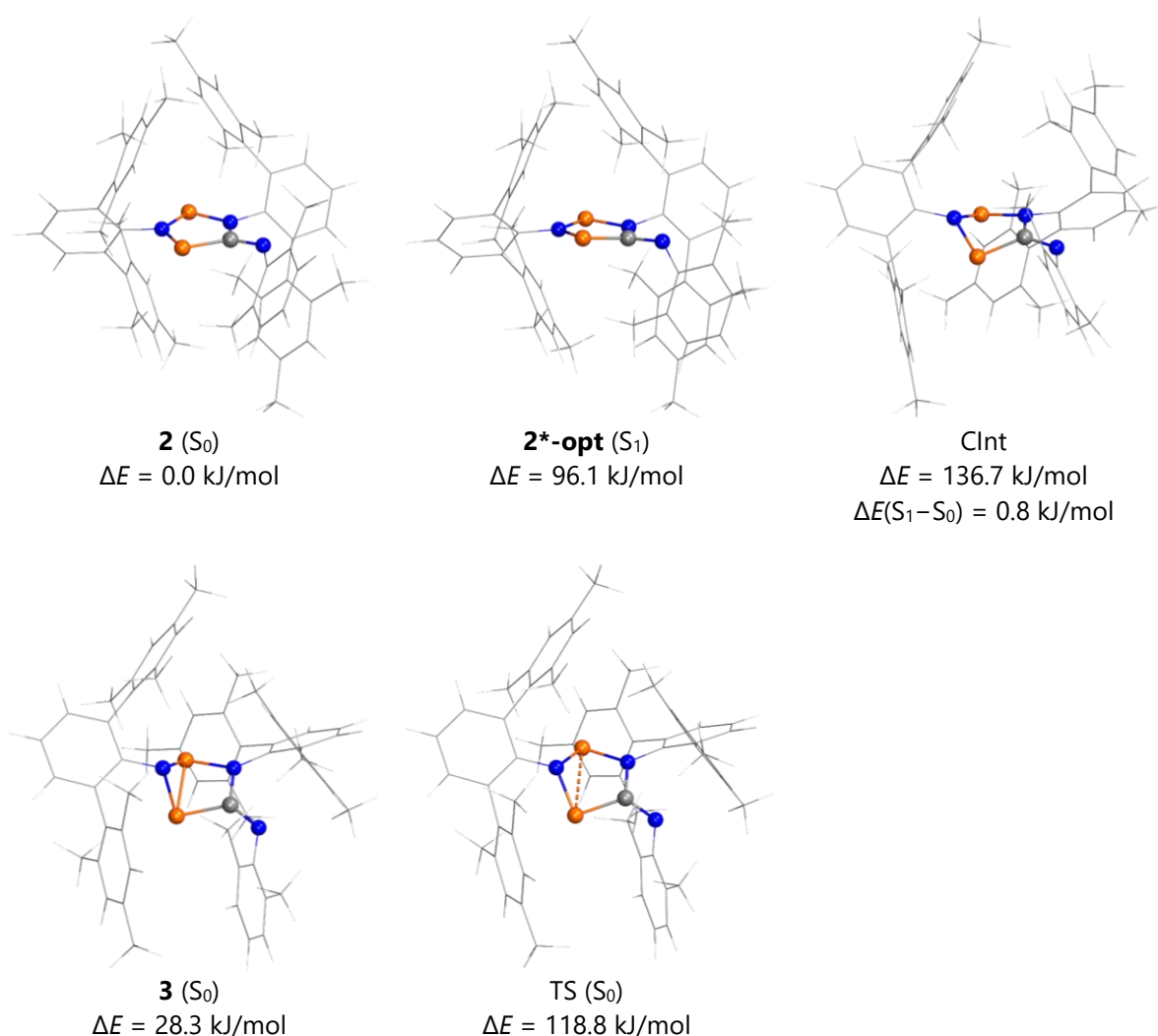
Figure S10. Active Space of CAS(2,2)/def2-TZVP computations (Natural Orbitals, NOs).



3.3 PES of [TerNP]₂CNDmp (2)

The relevant stationary points on the PES of the “real” system **2** were optimized at the (U)PBE-D3/def2-TZVP level of theory. The S₁ minimum structure (**2*^{-opt}**) as well as the Clnt were optimized using the TD-DFT/TDA method as described above. The ground-state PES agrees reasonably well with previous computations at the DLPNO-CCSD(T)/def2-TZVP//PBE-D3/def2-SVP level of theory.^[1]

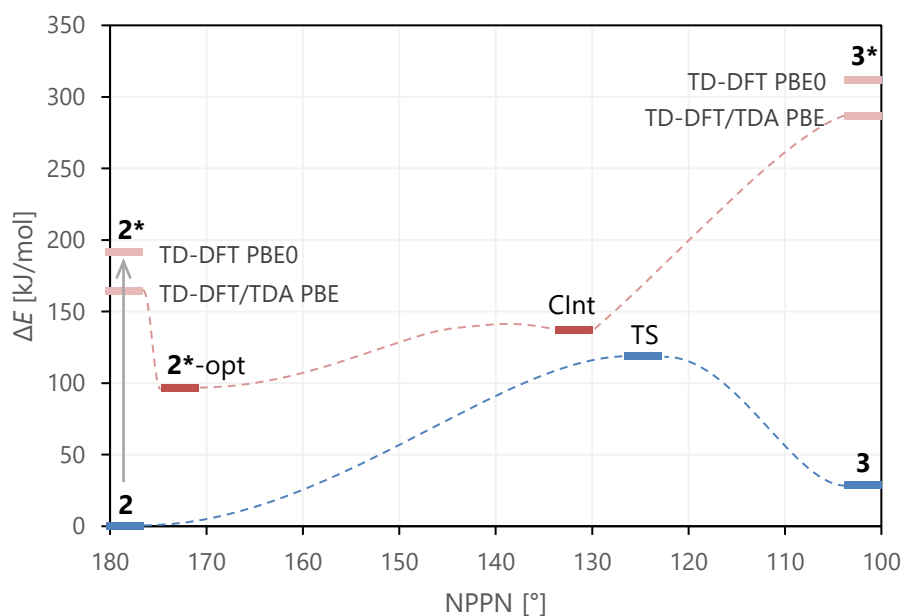
Figure S11. Structures of the relevant stationary points on the PES of **2** (UPBE-D3/def2-TZVP).



Note that the excitation energies obtained by the pure density functional PBE are somewhat too low; quite accurate results are obtained using the hybrid functional PBE0 (*cf.* UV-vis absorption spectra, section 3.5). Nonetheless, we opted to use the pure

functional for all structure optimizations due to its faster performance. The somewhat qualitative nature of the results should be kept in mind, though.

Figure S12. Schematic depiction of the PES of **2** (calculated points indicated as bars; UPBE-D3/def2-TZVP, TD-DFT/TDA for S_1 unless denoted otherwise).



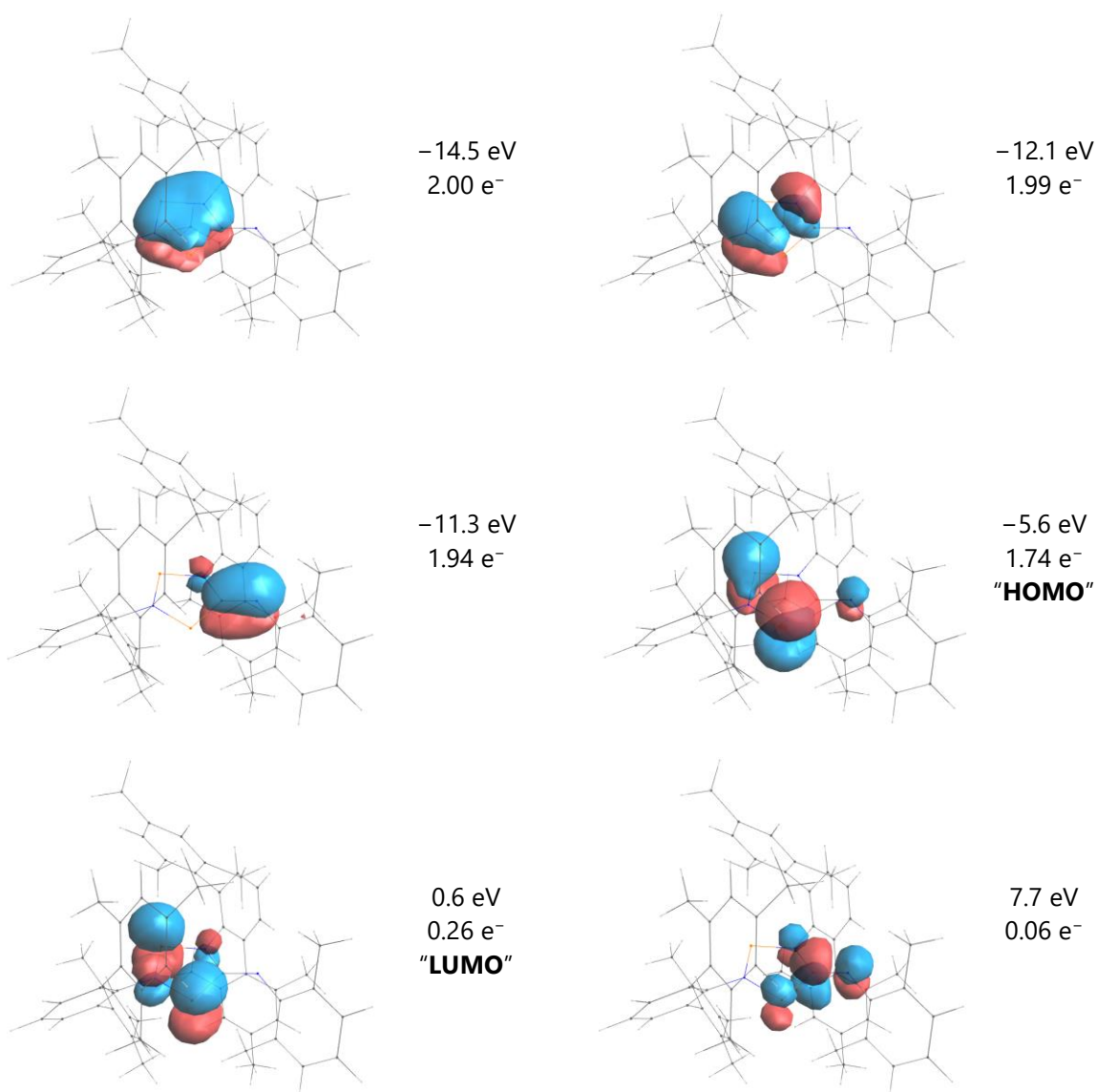
3.4 CASSCF wavefunction of biradical **2**

The electronic structure of biradical **2** was computed at the CAS(8,6)/def2-TZVP level of theory (using the optimized geometry at the PBE-D3/def2-TZVP level of theory). All π -type orbitals were placed in the active space. A summary of the results is given in Table S3 and Figure S13.

Table S3. Most important contributions ($c_i > 0.1$) to the CAS-CI expansion of the wavefunction of **2** (CAS(8,6)/def2-TZVP). The formal HOMO and LUMO are printed in bold for better readability.

Configuration	c_1	Configuration	c_2	Configuration	c_3
222 2 00	0.917	222 0 20	-0.347	220 2 02	-0.146

Figure S13. Active Space of the CAS(8,6)/def2-TZVP wavefunction of **2** (Natural Orbitals, NOs).



3.5 UV-vis absorption spectra

All UV-vis spectra were calculated using the optimized geometries at the PBE-D3/def2-TZVP level of theory (as described above). The spectra were plotted using Gaussian functions.

The ground-state UV-vis absorption spectra of **2** and **3** were computed using the TD-DFT method at the PBE0-D3/def2-TZVP level of theory (Figure S14, Figure S15).

Figure S14. Calculated UV-vis absorption spectrum (TD-DFT, PBE0-D3/def2-TZVP, 20 roots) of the biradical **2**. Half-width at half maximum set to 0.15 eV.

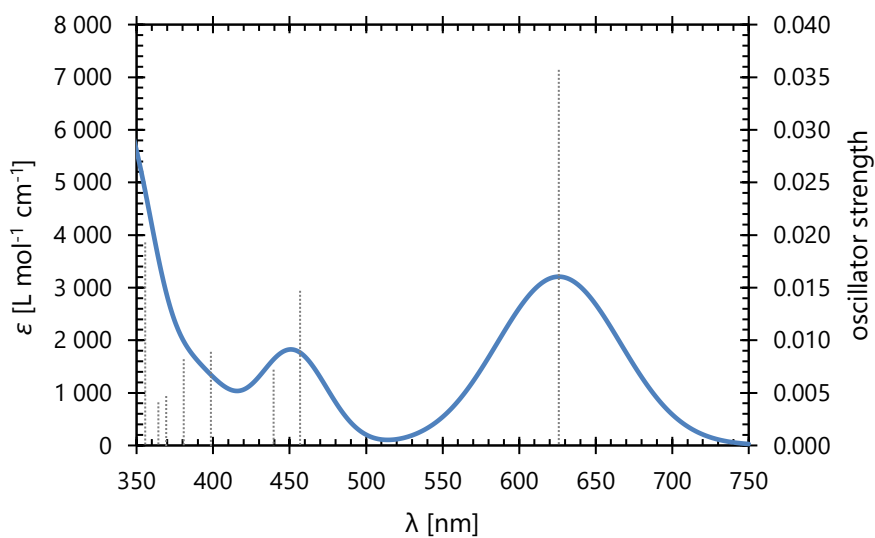
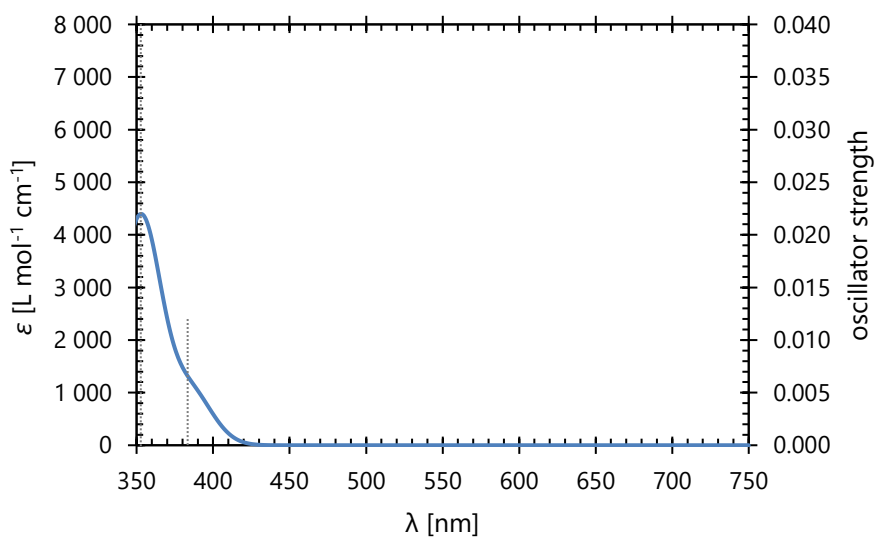


Figure S15. Calculated UV-vis absorption spectrum (TD-DFT, PBE0-D3/def2-TZVP, 20 roots) of the housane **3**. Half-width at half maximum set to 0.15 eV.



Transient UV-vis spectra were computed at the TD-DFT/TDA PBE0-D3/def2-TZVP level of theory (Figure S16 - Figure S18).

Figure S16. Calculated transient UV-vis absorption spectrum (TD-DFT/TDA, PBE0-D3/def2-TZVP, 80 roots) of **2*** (after vertical excitation). Half-width at half maximum set to 0.2 eV.

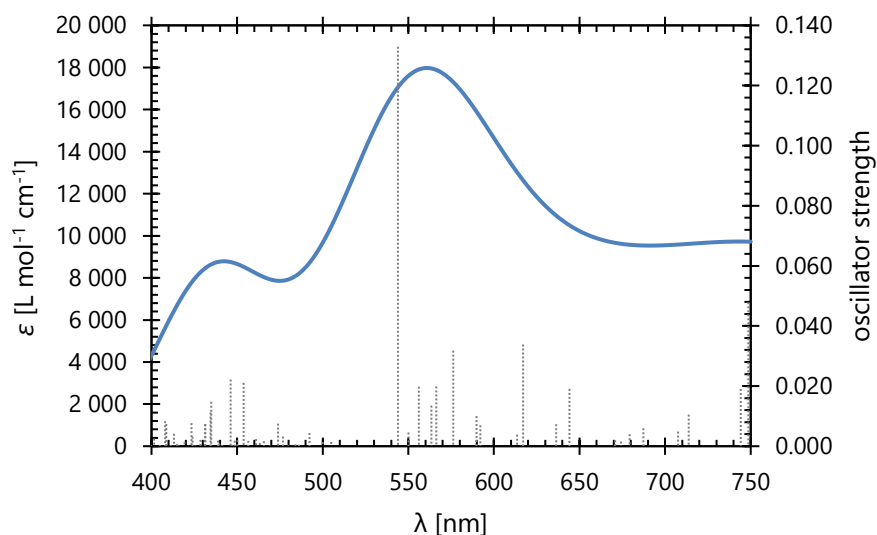


Figure S17. Calculated transient UV-vis absorption spectrum (TD-DFT/TDA, PBE0-D3/def2-TZVP, 30 roots) of **2*-opt** (S_1 optimized structure). Half-width at half maximum set to 0.2 eV.

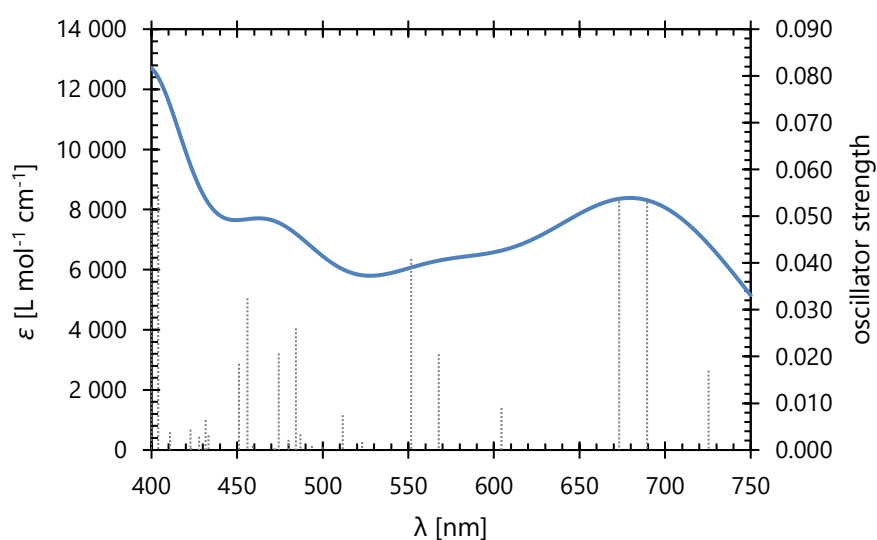


Figure S18. Calculated UV-vis absorption spectrum (TD-DFT/TDA, PBE0-D3/def2-TZVP, 30 roots) of a molecule at the conical intersection (CInt). Half-width at half maximum set to 0.2 eV.

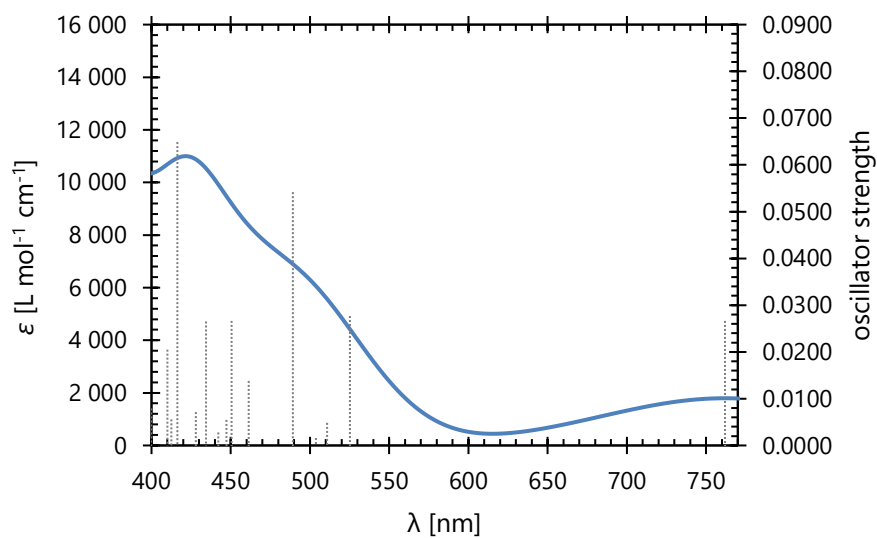
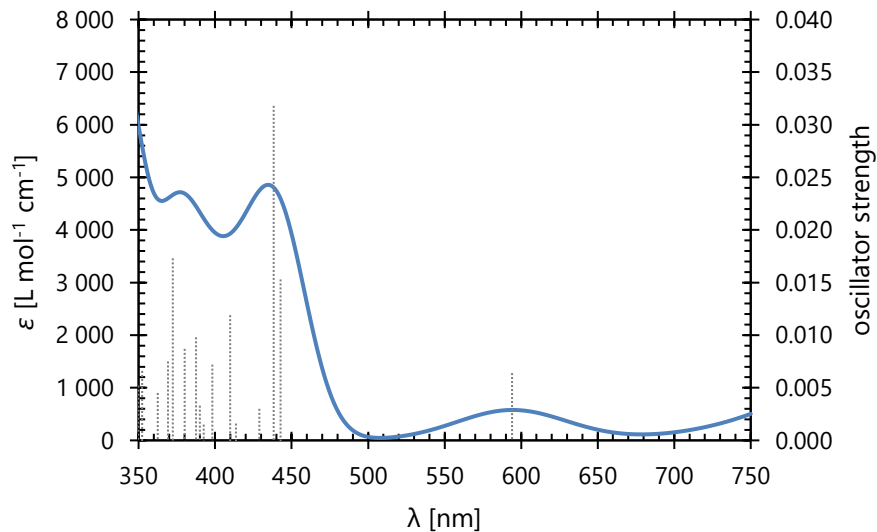


Figure S19. Calculated UV-vis absorption spectrum (TD-DFT, PBE0-D3/def2-TZVP, 20 roots) of a molecule on the ground-state MEP near the CInt (NPPN = 131.9°). Half-width at half maximum set to 0.15 eV.



3.6 Summary of calculated data

Table S4. Summary of calculated data. All energies in atomic units.

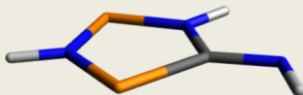
Structure	PG	$\langle S^2 \rangle$	E_{tot}	$\Delta U_{298\text{K}}^{[a]}$	$\Delta H_{298\text{K}}^{[b]}$	$\Delta G_{298\text{K}}^{[c]}$	$E_{\text{tot},2}^{[d]}$
model system (R = H)							
<i>structures optimized at (U)PBE-D3/def2-TZVP (TD-DFT/TDA for excited states)</i>							
2H	C _s	0	-886.4510	0.0603	0.0612	0.0244	
2H*	C _s	0	-886.3562	—	—	—	
2H*-TS	C _s	0	-886.3740	0.0577	0.0587	0.0208	
2H*-opt	C ₁	0	-886.3959	0.0679	0.0689	0.0316	
Clnt	C ₁	0	-886.3943	—	—	—	
TS	C ₁	0.84	-886.4008	0.0579	0.0589	0.0220	
3H	C ₁	0	-886.4344	0.0592	0.0601	0.0233	
<i>structures optimized at CAS(2,2)/def2-TZVP</i>							
2H	C _s	0	-884.5421	0.0664	0.0674	0.0314	
Clnt	C ₁	0	-884.4561 ^[e]	—	—	—	
TS	C ₁	0	-884.4990	0.0644	0.0653	0.0296	
3H	C ₁	0	-884.5201	0.0654	0.0664	0.0306	
<i>single-point energies, state-averaged CAS(2,2)/def2-TZVP</i>							<i>NEVPT2</i>
2H	C _s	0	-884.5238	—	—	—	-885.5633
2H*	C _s	0	-884.4107	—	—	—	-885.4628
Clnt	C ₁	0	-884.4561	—	—	—	-885.5014
TS	C ₁	0	-884.4747	—	—	—	-885.5159
3H	C ₁	0	-884.4979	—	—	—	-885.5472
3H*	C ₁	0	-884.3195	—	—	—	-885.4046
"real" system							
<i>structures optimized at (U)PBE-D3/def2-TZVP (TD-DFT/TDA for excited states)</i>							<i>PBE0-D3^[f]</i>
2	C ₁	0	-3052.2968	1.0404	1.0413	0.8772	-3052.5797
2*	C ₁	0	-3052.2344	—	—	—	-3052.5069
2*-opt	C ₁	0	-3052.2602	—	—	—	—

Structure	PG	$\langle S^2 \rangle$	E_{tot}	$\Delta U_{298\text{K}}^{[a]}$	$\Delta H_{298\text{K}}^{[b]}$	$\Delta G_{298\text{K}}^{[c]}$	$E_{\text{tot},2}^{[d]}$
Clnt	C ₁	0	-3052.2447	—	—	—	—
TS	C ₁	0.92	-3052.2516	1.0380	1.0390	0.8726	—
3	C ₁	0	-3052.2860	1.0401	1.0410	0.8791	-3052.5719
3*	C ₁	0	-3052.1876	—	—	—	-3052.4609

[a] Thermal correction to energy; [b] thermal correction to enthalpy; [c] thermal correction to Gibbs free energy; [d] single-point energies at indicated level of theory; [e] state-averaged CAS(2,2); [f] PBE0-D3/def2-TZVP, TD-DFT for excited states.

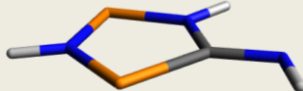
3.7 Optimized structures (.xyz-files)

3.7.1 2H


9				
2H, PBE-D3/def2-TZVP				
C	0.09612	1.17409	0.00001	
N	0.05053	2.46406	-0.00001	
N	-1.13090	0.46012	0.00001	
N	0.43138	-1.36018	-0.00001	
P	1.49356	0.00058	0.00003	
P	-1.23279	-1.21559	0.00001	
H	0.83307	-2.29670	-0.00002	
H	0.99035	2.87036	-0.00001	
H	-1.96636	1.04749	-0.00001	

9			
2H, CAS(2,2)/def2-TZVP			
C	-1.08782	-0.29738	0.06305
N	-2.29639	-0.64155	0.00016
N	-0.07842	-1.23748	0.00876
N	1.18994	0.78123	0.21975
P	-0.37580	1.38214	0.22927
P	1.54820	-0.83661	0.08814
H	-2.91736	0.14064	0.05192
H	-0.37803	-2.18370	-0.08262
H	1.94778	1.42346	0.29567

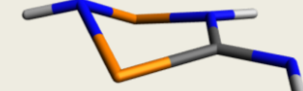
3.7.2 2H*-TS

9				
2H*-TS, TD-DFT/TDA, PBE-D3/def2-TZVP				
C	0.09360	1.07755	-0.00016	
N	-0.00035	2.49863	-0.00046	
N	-1.09420	0.48847	0.00001	
N	0.42788	-1.38542	-0.00025	
P	1.50715	0.03242	0.00007	
P	-1.26631	-1.24506	0.00033	
H	0.84130	-2.31337	-0.00001	
H	0.95901	2.87510	0.00047	
H	-1.90312	1.11591	-0.00000	

3.7.3 2H*-opt

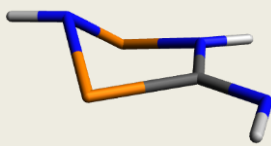
9				
2H*-opt, TD-DFT/TDA, PBE-D3/def2-TZVP				
C	0.19308	1.05745	0.18293	
N	0.28820	2.46291	0.39002	
N	-1.02788	0.53476	-0.01606	
N	0.41348	-1.39840	-0.02767	
P	1.53378	-0.06827	0.26764	
P	-1.26005	-1.15736	-0.22074	
H	0.79048	-2.34039	-0.03714	
H	0.45920	2.88724	-0.53649	
H	-1.82535	1.16630	-0.00249	

3.7.4 CInt (model system)

9				
CInt, TD-DFT/TDA, PBE-D3/def2-TZVP				
C	-1.10293	-0.23515	0.10992	
N	-2.31384	-0.69484	0.06815	
N	-0.08013	-1.25933	0.08965	
N	1.31898	0.74562	0.57833	
P	-0.40271	1.40791	-0.02767	
P	1.43001	-0.67988	-0.22397	
H	-2.99348	0.07478	0.02231	
H	-0.39260	-2.21897	-0.06274	
H	2.08133	1.38949	0.35096	

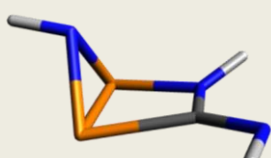
9			
CInt, state-averaged CAS(2,2)/def2-TZVP			
C	-1.10083	-0.26591	0.07576
N	-2.29022	-0.64774	0.10949
N	-0.08382	-1.25671	0.07946
N	1.24043	0.73783	0.51883
P	-0.36255	1.38685	-0.17758
P	1.41826	-0.69514	-0.18164
H	-2.93026	0.12207	0.08256
H	-0.36719	-2.19917	-0.07622
H	2.01134	1.36732	0.45381

3.7.5 TS (model system)

9				
TS, UPBE-D3/def2-TZVP				
C	-1.08784	-0.33152	0.06330	
N	-2.33249	-0.64336	0.10598	
N	-0.08297	-1.29398	0.07528	
N	1.20867	0.75924	0.60141	
P	-0.30946	1.34347	-0.12243	
P	1.45160	-0.66491	-0.38794	
H	-2.92191	0.19673	0.06933	
H	-0.34904	-2.27491	0.00681	
H	1.96806	1.43888	0.49319	

9			
TS, CAS(2,2)/def2-TZVP			
C	-1.08207	-0.33980	0.07226
N	-2.29667	-0.62474	0.11588
N	-0.07871	-1.28865	0.10079
N	1.17589	0.75582	0.55497
P	-0.30012	1.33519	-0.13923
P	1.42253	-0.66530	-0.39025
H	-2.88010	0.18760	0.07118
H	-0.34589	-2.24112	-0.00870
H	1.92975	1.41065	0.52802

3.7.6 3H

9				
3H, PBE-D3/def2-TZVP				
C	0.03643	1.26551	-0.05106	
N	0.08485	2.53545	-0.00943	
N	-1.12751	0.50313	-0.07388	
N	0.50251	-0.87944	1.34265	
P	1.34725	-0.13156	-0.09175	
P	-0.57555	-1.15254	-0.04585	
H	1.00086	-1.74055	1.61030	
H	1.05035	2.87933	-0.02951	
H	-2.00997	0.87214	0.28335	

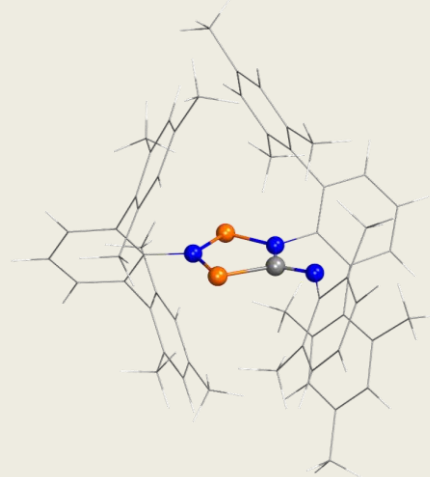
9			
3H, CAS(2,2)/def2-TZVP			
C	-1.10577	-0.36863	-0.07398
N	-2.29031	-0.57869	0.24067
N	-0.12030	-1.33575	-0.20168
N	1.08469	0.69081	0.69543
P	-0.12364	1.18143	-0.49961
P	1.30389	-0.47134	-0.56026
H	-2.83364	0.26165	0.25218
H	-0.20120	-2.20758	0.27343
H	1.82339	1.35667	0.80954

3.7.7 Biradical 2

121

Energy: -1915344.5159108

C	-5.93021	-0.33691	3.26823
C	-4.44306	-0.54109	3.16020
C	-3.91423	-1.61302	2.43693
C	-3.54942	0.33095	3.79013
C	-5.36467	-3.17780	-1.91506
C	-2.53761	-1.84111	2.34522
C	-4.78906	-0.91935	-0.94199
C	-2.16607	0.13215	3.74165
C	-4.69330	-1.83313	-1.99457
C	-2.01566	-3.02110	1.57628
C	-4.24841	1.25506	0.19878
C	-1.65591	-0.96752	3.01489
C	-1.24673	1.08402	4.46099
C	-4.11448	0.30560	-0.96109
C	0.21442	-1.91489	4.30342
C	0.21361	-4.95435	-0.52814
C	-3.93945	-1.46850	-3.11480
C	-0.20192	-1.29735	3.11358
C	1.54469	-2.26197	4.50856
C	-3.32745	0.62997	-2.08375
C	1.48370	-5.11186	-2.69250
C	1.07609	-4.34933	-1.59893
C	-3.26860	-0.24392	-3.18918
C	0.75903	-1.02934	2.11486
C	2.29212	-4.56681	-3.69233
C	-2.61577	1.93982	-2.10954
C	-3.20504	3.01499	-2.78562
C	1.47163	-2.98538	-1.50198
C	2.48607	-1.96206	3.52843
C	-0.81030	4.68632	1.25699
C	0.53236	-1.13753	-0.36564
C	-2.51051	0.12438	-4.43650
C	2.12382	-1.33499	2.32897
C	2.70501	-3.24355	-3.58039
C	-2.62403	4.28057	-2.77300
C	-1.39966	2.15709	-1.42264
C	2.32082	-2.43371	-2.50176
C	2.79274	1.50078	1.94781
C	-1.43714	4.48280	-2.07586
C	-0.79874	3.43347	-1.39631
C	2.86302	-1.03253	-2.43538
C	0.48065	4.41297	0.53027
C	3.22649	-0.95110	1.40464
C	3.55241	0.41227	1.24161
C	0.49193	3.75183	-0.71497
C	1.69541	4.83506	1.08506
C	3.76096	-3.41453	0.99578
C	4.03616	-1.94596	0.80786
C	4.64800	0.75845	0.43982
C	1.71329	3.52858	-1.38770
C	2.91528	4.62904	0.43706
C	1.74335	2.86475	-2.73708
C	5.12258	-1.55102	0.02287
C	2.90039	3.96830	-0.79625
C	5.44044	-0.20480	-0.18584



C	4.21283	5.08131	1.05007
C	6.58014	0.19072	-1.08523
H	-6.33021	-0.81962	4.17445
H	-6.18672	0.73026	3.32826
H	-6.45995	-0.77064	2.40836
H	-6.27697	-3.13707	-1.30357
H	-4.59136	-2.30234	1.92629
H	-3.93828	1.19109	4.34236
H	-5.63328	-3.55469	-2.91153
H	-5.40600	-1.16311	-0.07398
H	-4.69429	-3.92220	-1.45500
H	-5.14717	1.02842	0.78536
H	-1.81061	1.92914	4.87672
H	-1.53210	-3.75031	2.24528
H	-2.82956	-3.53014	1.04360
H	-0.53722	-2.12682	5.06581
H	0.16285	-6.04606	-0.63882
H	-4.30302	2.30045	-0.13504
H	-0.71242	0.58865	5.28547
H	0.59708	-4.71059	0.47371
H	-3.38915	1.17248	0.88392
H	-1.25252	-2.72845	0.84266
H	-0.47347	1.48653	3.78775
H	-3.86987	-2.15740	-3.96084
H	1.16385	-6.15500	-2.75541
H	1.85039	-2.74907	5.43576
H	-0.81364	-4.56037	-0.56802
H	-4.14712	2.84300	-3.30888
H	2.61080	-5.17573	-4.53981
H	-1.44389	5.39603	0.70360
H	-1.40762	3.77052	1.38618
H	-0.61453	5.10777	2.25144
H	2.36634	1.15274	2.89805
H	-2.45287	-0.72990	-5.12313
H	-3.09760	5.10881	-3.30233
H	1.95930	1.88234	1.33347
H	3.54058	-2.18886	3.69075
H	-2.99522	0.95752	-4.96884
H	3.36255	-2.81388	-4.34084
H	3.88068	-1.00118	-2.85060
H	-1.48452	0.44571	-4.20539
H	3.44470	2.35831	2.15579
H	2.24474	-0.33232	-3.02289
H	-0.96792	5.46803	-2.05868
H	1.68268	5.34313	2.05315
H	2.68751	-3.59984	1.11723
H	4.27992	-3.80934	1.88406
H	2.90177	-0.64535	-1.41106
H	4.89167	1.81728	0.31684
H	4.11371	-3.98440	0.12581
H	1.34535	1.83914	-2.68567
H	1.12398	3.41109	-3.46487
H	4.83344	4.22096	1.34926
H	4.04216	5.69526	1.94434
H	5.72963	-2.32463	-0.45532
H	2.76859	2.81146	-3.12494
H	3.84222	3.79439	-1.32382
H	4.80774	5.67145	0.33739
H	6.96572	1.18799	-0.83152
H	6.25458	0.22191	-2.13820

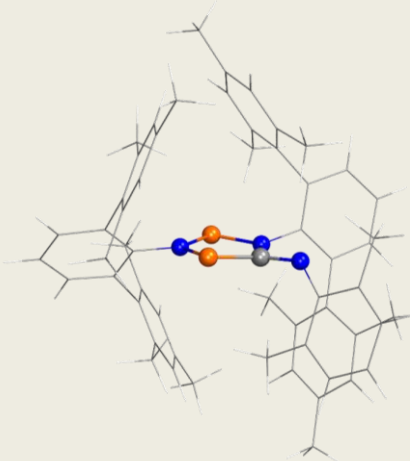
H	7.41022	-0.52705	-1.02397
N	1.09880	-2.30129	-0.34551
N	0.33239	-0.44187	0.86877
N	-0.75007	1.03971	-0.77783
P	-0.18259	-0.27026	-1.76888
P	-0.50978	1.03294	0.88024

3.7.8 2*-opt

121

Energy: -1915318.0274086

C	-5.95577	-0.56425	3.17922
C	-4.46975	-0.76433	3.04671
C	-3.94654	-1.82579	2.30830
C	-3.57004	0.10023	3.67968
C	-5.96906	-2.74194	-2.00530
C	-2.56828	-2.05160	2.19852
C	-5.05548	-0.65283	-0.92163
C	-2.18785	-0.08382	3.59792
C	-5.16131	-1.47230	-2.04868
C	-2.07133	-3.26363	1.46154
C	-4.18792	1.35371	0.31873
C	-1.68127	-1.16508	2.83913
C	-1.26705	0.85183	4.33573
C	-4.26835	0.50242	-0.91761
C	0.18370	-2.14265	4.08627
C	0.51224	-5.19309	-0.40333
C	-4.47800	-1.09026	-3.20722
C	-0.21771	-1.46680	2.92420
C	1.52090	-2.42896	4.33693
C	-3.56327	0.85109	-2.08839
C	2.39666	-5.18911	-2.05632
C	1.50369	-4.48819	-1.27078
C	-3.68585	0.06084	-3.25171
C	0.76765	-1.09418	1.97836
C	3.33276	-4.51927	-2.85798
C	-2.75697	2.10441	-2.09878
C	-3.28584	3.22386	-2.75200
C	1.51414	-3.02205	-1.27372
C	2.48238	-2.01586	3.42350
C	-0.55446	4.82610	1.23441
C	0.18777	-1.15514	-0.42674
C	-2.94654	0.41586	-4.51408
C	2.13569	-1.34290	2.24160
C	3.37302	-3.11644	-2.86039
C	-2.65036	4.46101	-2.70252
C	-1.52629	2.22216	-1.39951
C	2.51493	-2.34242	-2.09792
C	2.85808	1.50983	2.09344
C	-1.44897	4.57397	-2.00541
C	-0.86117	3.47442	-1.36641
C	2.62931	-0.85177	-2.16234
C	0.64589	4.43225	0.41530
C	3.26766	-0.90075	1.37681
C	3.60664	0.46992	1.30774
C	0.49498	3.69969	-0.78239
C	1.93029	4.78172	0.83972
C	3.88995	-3.34143	0.93099



C	4.10208	-1.85911	0.76047
C	4.70460	0.85862	0.53388
C	1.62996	3.32282	-1.52719
C	3.07202	4.42368	0.11285
C	1.48447	2.58066	-2.82719
C	5.18830	-1.42210	-0.00626
C	2.89929	3.68411	-1.05892
C	5.49286	-0.06793	-0.15447
C	4.44370	4.81965	0.59046
C	6.62495	0.38533	-1.03604
H	-6.31708	-0.91343	4.15979
H	-6.22864	0.49800	3.09549
H	-6.50629	-1.12116	2.40848
H	-6.84608	-2.63847	-1.35053
H	-4.62850	-2.51676	1.80580
H	-3.95422	0.94534	4.25775
H	-6.31798	-3.03275	-3.00578
H	-5.60560	-0.91468	-0.01452
H	-5.36573	-3.57686	-1.61268
H	-5.04776	1.17041	0.97429
H	-1.83465	1.66926	4.79918
H	-1.57860	-3.96691	2.15254
H	-2.90557	-3.79098	0.98006
H	-0.58845	-2.43639	4.79958
H	0.59171	-6.28120	-0.52294
H	-4.15503	2.42387	0.07149
H	-0.70844	0.33004	5.12753
H	0.66024	-4.93853	0.65722
H	-3.28051	1.12151	0.90043
H	-1.32968	-3.01272	0.69222
H	-0.52020	1.29625	3.66043
H	-4.55665	-1.71057	-4.10440
H	2.37069	-6.28058	-2.04759
H	1.81269	-2.95436	5.24764
H	-0.51278	-4.87455	-0.64373
H	-4.23874	3.11277	-3.27314
H	4.03277	-5.08509	-3.47362
H	-1.22137	5.50536	0.68326
H	-1.15849	3.94492	1.50235
H	-0.24716	5.32365	2.16352
H	2.46434	1.10194	3.03449
H	-3.11075	-0.34555	-5.28777
H	-3.08390	5.32841	-3.20186
H	2.00358	1.90902	1.52322
H	3.54029	-2.19571	3.61955
H	-3.26228	1.38911	-4.91759
H	4.11570	-2.60684	-3.47839
H	3.57582	-0.57080	-2.64185
H	-1.86337	0.48750	-4.32732
H	3.51191	2.35916	2.32910
H	1.79900	-0.42284	-2.73905
H	-0.91706	5.52711	-1.97702
H	2.04176	5.34948	1.76796
H	2.84195	-3.59184	1.12940
H	4.47938	-3.72300	1.78037
H	2.59962	-0.38420	-1.17045
H	4.95762	1.92016	0.48303
H	4.21648	-3.88577	0.03559
H	0.93603	1.63595	-2.69310
H	0.91442	3.17257	-3.55992

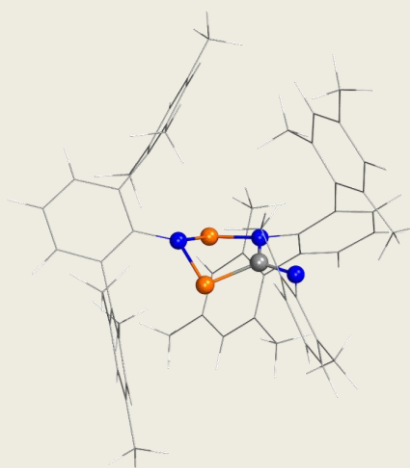
H	4.68895	4.34154	1.55248
H	4.51433	5.90645	0.74823
H	5.81005	-2.16976	-0.50642
H	2.46709	2.34926	-3.25840
H	3.77693	3.39190	-1.64200
H	5.21791	4.53223	-0.13386
H	7.12719	1.27159	-0.62287
H	6.25541	0.66050	-2.03786
H	7.37475	-0.40653	-1.16916
N	0.59932	-2.46571	-0.50088
N	0.33733	-0.45718	0.74645
N	-0.96595	1.07680	-0.77394
P	-0.82574	-0.45851	-1.66558
P	-0.36068	1.14345	0.82797

3.7.9 CInt

121

Energy: -1915308.3095368

C	1.49551	-3.36731	-5.52971
C	0.93434	-3.39476	-4.13207
C	1.63729	-3.99225	-3.08236
C	-0.30559	-2.81848	-3.83829
C	4.43966	3.75474	4.17525
C	1.15893	-3.99598	-1.76550
C	3.73445	4.00550	1.76081
C	-0.82302	-2.79437	-2.53794
C	3.38256	3.82217	3.10470
C	1.94929	-4.72637	-0.70986
C	3.22218	4.20054	-0.68837
C	-0.06403	-3.34708	-1.48121
C	-2.20979	-2.25643	-2.30291
C	2.77967	4.04996	0.74329
C	-1.11276	-4.62768	0.34554
C	3.08082	-0.61520	-2.09786
C	2.02699	3.69853	3.41358
C	-0.66482	-3.38021	-0.11289
C	-1.81971	-4.76199	1.53619
C	1.41205	3.88904	1.07492
C	5.27361	-0.95269	-0.93158
C	3.87506	-1.01749	-0.88147
C	1.03221	3.73368	2.42710
C	-0.90644	-2.23286	0.68928
C	6.06753	-1.35501	0.13981
C	0.35666	4.00776	0.02149
C	0.06476	5.30257	-0.42894
C	3.26652	-1.51090	0.30509
C	-2.11326	-3.62366	2.27819
C	-0.54649	1.67048	-3.68401
C	1.06102	-0.72015	0.31409
C	-0.41390	3.61239	2.82923
C	-1.66886	-2.35264	1.88060
C	5.45920	-1.86289	1.28740
C	-0.98476	5.55521	-1.30594
C	-0.40864	2.90857	-0.46553
C	4.06937	-1.96390	1.38436
C	-4.35853	-1.22415	1.61814
C	-1.75937	4.48352	-1.74431



C	-1.49523	3.16548	-1.35074
C	3.43137	-2.52671	2.62374
C	-1.95106	1.49520	-3.17058
C	-2.07968	-1.21104	2.76287
C	-3.41069	-0.72381	2.67672
C	-2.37157	2.12426	-1.97500
C	-2.87108	0.73016	-3.89497
C	0.19611	-1.20310	3.90007
C	-1.22084	-0.72118	3.77203
C	-3.83402	0.26113	3.57104
C	-3.70036	1.95010	-1.51939
C	-4.19003	0.54787	-3.46550
C	-4.19639	2.63399	-0.27150
C	-1.69426	0.26454	4.64857
C	-4.57732	1.15469	-2.26653
C	-2.99105	0.77459	4.56593
C	-5.15389	-0.29921	-4.25354
C	-3.47381	1.84409	5.50988
H	2.12907	-4.24359	-5.72679
H	0.69645	-3.34368	-6.28421
H	2.11982	-2.47244	-5.68717
H	5.14552	4.59523	4.09691
H	2.59604	-4.47671	-3.28980
H	-0.90451	-2.39319	-4.64910
H	3.99547	3.77422	5.17961
H	4.79047	4.10802	1.49471
H	5.03053	2.82922	4.08809
H	4.31292	4.30971	-0.74940
H	-2.73694	-2.12583	-3.25590
H	1.63720	-5.78178	-0.64405
H	3.02053	-4.71886	-0.95377
H	-0.91972	-5.50296	-0.27709
H	3.70469	-0.69862	-2.99891
H	2.75988	5.06956	-1.17846
H	-2.79994	-2.93699	-1.67165
H	2.19167	-1.24502	-2.23517
H	2.93507	3.31536	-1.27903
H	1.81642	-4.27271	0.27847
H	-2.19870	-1.27612	-1.80291
H	1.72622	3.57670	4.45818
H	5.74356	-0.58519	-1.84739
H	-2.15998	-5.74337	1.87077
H	2.73434	0.42822	-2.02581
H	0.66467	6.12756	-0.03850
H	7.15509	-1.29308	0.07318
H	-0.29931	2.73338	-3.82724
H	0.19051	1.26773	-2.97192
H	-0.41121	1.15068	-4.64145
H	-4.50730	-2.31215	1.67854
H	-0.53448	3.79225	3.90621
H	-1.20479	6.57163	-1.63507
H	-3.97336	-1.01764	0.60574
H	-2.69035	-3.70173	3.20181
H	-1.05062	4.32241	2.28260
H	6.07093	-2.20183	2.12722
H	2.59989	-3.20076	2.36988
H	-0.80367	2.60000	2.62639
H	-5.33765	-0.73611	1.71149
H	4.16730	-3.07682	3.22567
H	-2.58712	4.65409	-2.43627

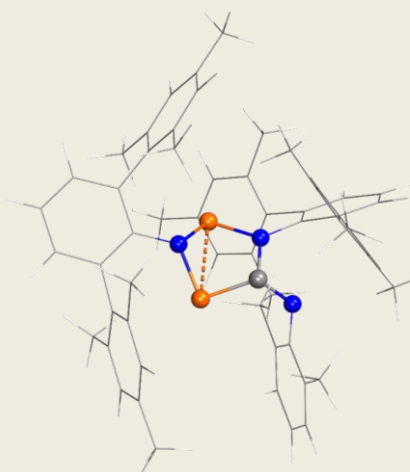
H	-2.54502	0.26836	-4.83161
H	0.85101	-0.63910	3.21342
H	0.29643	-2.26626	3.64540
H	3.00683	-1.73217	3.25688
H	-4.85845	0.63663	3.49172
H	0.57404	-1.04577	4.91950
H	-3.56880	2.39204	0.60056
H	-4.18029	3.72940	-0.37470
H	-6.19037	0.04135	-4.12099
H	-5.11392	-1.35219	-3.92853
H	-1.02190	0.63870	5.42588
H	-5.22624	2.32786	-0.04385
H	-5.60409	1.02833	-1.91077
H	-4.92009	-0.28132	-5.32730
H	-4.42836	1.56338	5.97997
H	-3.64454	2.79424	4.97932
H	-2.74365	2.03366	6.30798
N	1.87554	-1.71362	0.38917
N	-0.36100	-0.95599	0.30705
N	-0.09352	1.58330	-0.10701
P	1.52422	1.01788	0.58172
P	-1.21709	0.51974	0.56634

3.7.10 TS

121

Energy: -1915312.1294820

C	-3.55692	-3.18512	4.44547
C	-2.59468	-3.28408	3.29284
C	-2.99775	-3.80816	2.06212
C	-1.27924	-2.82496	3.40855
C	-5.56615	3.47871	-1.24441
C	-2.13976	-3.86464	0.95799
C	-3.88912	3.32313	0.63633
C	-0.38663	-2.86030	2.33161
C	-4.17551	3.64320	-0.69622
C	-2.63963	-4.47164	-0.32625
C	-2.31306	3.04542	2.58462
C	-0.82709	-3.35975	1.08704
C	1.04038	-2.43293	2.53204
C	-2.59189	3.39924	1.14831
C	0.54484	-4.79538	-0.36701
C	-3.31924	-0.42512	1.39483
C	-3.12882	4.09557	-1.50593
C	0.15343	-3.49218	-0.02766
C	1.52976	-5.04506	-1.31752
C	-1.53912	3.78798	0.28817
C	-5.32432	-0.32004	-0.10138
C	-3.96056	-0.60260	0.04586
C	-1.81332	4.17630	-1.03880
C	0.76768	-2.40490	-0.69868
C	-5.98250	-0.49278	-1.31660
C	-0.14529	3.81203	0.81387
C	0.32230	5.02570	1.32639
C	-3.24590	-1.07684	-1.08619
C	2.15951	-3.96989	-1.93478
C	1.28660	0.90491	3.59697
C	-0.98199	-0.66351	-0.64460



C	-0.70116	4.57649	-1.96948
C	1.79384	-2.64988	-1.64113
C	-5.27341	-0.97654	-2.41797
C	1.59158	5.14700	1.88553
C	0.68576	2.65330	0.85386
C	-3.91663	-1.28554	-2.32012
C	4.51406	-2.03179	-0.81273
C	2.38966	4.01001	1.96007
C	1.96383	2.76752	1.47376
C	-3.15391	-1.80730	-3.50379
C	2.58166	0.76731	2.84387
C	2.52993	-1.55060	-2.32875
C	3.85942	-1.26615	-1.93088
C	2.87625	1.62001	1.75665
C	3.52079	-0.19891	3.21911
C	0.52985	-1.10024	-3.83027
C	1.93716	-0.82415	-3.38217
C	4.54719	-0.23041	-2.56453
C	4.11799	1.51016	1.08682
C	4.74289	-0.34084	2.55644
C	4.44941	2.40166	-0.07827
C	2.66798	0.20440	-3.99030
C	5.02341	0.53094	1.49821
C	3.96435	0.52900	-3.58701
C	5.71873	-1.41648	2.94922
C	4.71603	1.67036	-4.21670
H	-4.28974	-4.00385	4.42901
H	-3.03270	-3.20865	5.41096
H	-4.12334	-2.24002	4.40310
H	-6.32637	3.79336	-0.51501
H	-4.02069	-4.17780	1.94832
H	-0.92794	-2.43913	4.36987
H	-5.70650	4.06110	-2.16495
H	-4.69906	2.99224	1.29205
H	-5.75943	2.42011	-1.48137
H	-3.23481	2.74866	3.10138
H	1.23343	-2.21559	3.58978
H	-2.45181	-5.55708	-0.35329
H	-3.72331	-4.32154	-0.42578
H	0.06770	-5.62434	0.15802
H	-4.05121	-0.62008	2.19133
H	-1.86807	3.89482	3.12460
H	1.74166	-3.21654	2.20760
H	-2.46721	-1.09775	1.54263
H	-1.59322	2.21619	2.66545
H	-2.14593	-4.02094	-1.19429
H	1.29010	-1.53122	1.95573
H	-3.33792	4.36927	-2.54361
H	-5.87864	0.03461	0.77112
H	1.81351	-6.06929	-1.56355
H	-2.95446	0.60437	1.52499
H	-0.34591	5.88813	1.27841
H	-7.04699	-0.26827	-1.40267
H	1.10683	1.94877	3.89300
H	0.43074	0.59984	2.97355
H	1.28647	0.28051	4.49966
H	4.61335	-3.10061	-1.05069
H	-1.10162	4.99252	-2.90308
H	1.94236	6.10239	2.27670
H	3.91845	-1.96444	0.11048

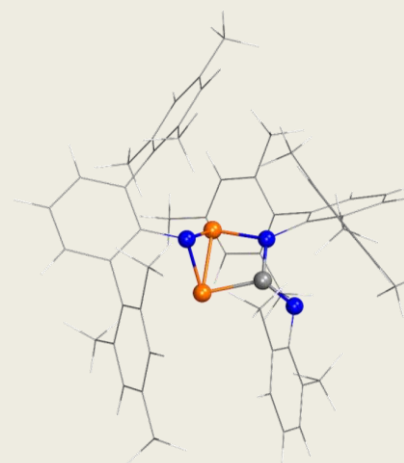
H	2.94291	-4.13659	-2.67636
H	-0.02846	5.31541	-1.51244
H	-5.78212	-1.12901	-3.37280
H	-2.51206	-2.65285	-3.21536
H	-0.08105	3.70181	-2.23000
H	5.51266	-1.62973	-0.60147
H	-3.83731	-2.12699	-4.30156
H	3.37060	4.05791	2.43734
H	3.29501	-0.85482	4.06377
H	-0.18440	-0.50326	-3.24061
H	0.25304	-2.15375	-3.69736
H	-2.48240	-1.03980	-3.91981
H	5.56630	-0.00038	-2.24197
H	0.39377	-0.82656	-4.88533
H	3.73582	2.24258	-0.90332
H	4.39496	3.46675	0.18683
H	6.75848	-1.08051	2.82992
H	5.59145	-2.31047	2.31662
H	2.20228	0.77200	-4.80053
H	5.45651	2.18693	-0.45853
H	5.97925	0.44422	0.97425
H	5.57375	-1.73016	3.99192
H	5.73821	1.37404	-4.49460
H	4.80490	2.51504	-3.51469
H	4.20701	2.03727	-5.11765
N	-1.90715	-1.48306	-1.00876
N	0.34588	-1.05793	-0.45419
N	0.26013	1.41172	0.33626
P	-1.19805	1.15788	-0.63718
P	1.42371	0.34653	-0.48198

3.7.11 Housane 3

121

Energy: -1915333.7499003

C	-3.44504	-2.83493	4.66349
C	-2.42877	-3.01993	3.56921
C	-2.73271	-3.76185	2.42382
C	-1.16679	-2.42381	3.64725
C	-6.14894	2.94625	-0.97213
C	-1.82966	-3.89859	1.36375
C	-4.26560	2.84880	0.71265
C	-0.22878	-2.54031	2.61562
C	-4.71505	3.16063	-0.57287
C	-2.22551	-4.70907	0.15782
C	-2.48706	2.68362	2.49157
C	-0.57054	-3.26476	1.45398
C	1.14139	-1.94327	2.78263
C	-2.92538	2.99912	1.08601
C	0.96963	-4.77645	0.25902
C	-3.32849	-0.48149	1.11461
C	-3.78464	3.66103	-1.49085
C	0.46121	-3.47660	0.40100
C	1.99896	-5.07092	-0.62882
C	-2.00026	3.47758	0.13565
C	-5.25403	-0.57578	-0.51062
C	-3.90034	-0.79975	-0.23737
C	-2.44003	3.83713	-1.15877



C	1.00802	-2.44713	-0.40192
C	-5.81533	-0.91644	-1.74036
C	-0.59114	3.73074	0.55684
C	-0.27083	5.05275	0.89278
C	-3.10077	-1.38747	-1.24766
C	2.55879	-4.04271	-1.38146
C	1.39534	1.41146	3.59542
C	-0.87034	-0.85805	-0.73508
C	-1.47265	4.36466	-2.18272
C	2.08079	-2.73131	-1.28030
C	-5.01817	-1.50952	-2.71938
C	0.98487	5.40439	1.37696
C	0.39287	2.71415	0.69695
C	-3.66344	-1.76357	-2.48894
C	4.67521	-1.76544	-0.41871
C	1.93284	4.40135	1.55094
C	1.66173	3.06514	1.22870
C	-2.80627	-2.41368	-3.53731
C	2.62402	1.31298	2.73157
C	2.75144	-1.66152	-2.07094
C	4.01267	-1.18911	-1.64025
C	2.73113	2.07828	1.55005
C	3.69689	0.50282	3.11501
C	0.87389	-1.70323	-3.77451
C	2.16172	-1.13912	-3.24111
C	4.62876	-0.16016	-2.35535
C	3.91738	2.03606	0.78524
C	4.88159	0.44499	2.37313
C	4.05047	2.83707	-0.48091
C	2.81110	-0.10121	-3.91987
C	4.97057	1.22300	1.21523
C	4.03518	0.41483	-3.48496
C	6.01661	-0.44469	2.80275
C	4.69145	1.56607	-4.19734
H	-4.10381	-3.70989	4.75308
H	-2.96345	-2.66257	5.63602
H	-4.08678	-1.96293	4.45589
H	-6.79791	2.83490	-0.09275
H	-3.71440	-4.23627	2.33952
H	-0.89387	-1.86125	4.54462
H	-6.52748	3.78284	-1.57702
H	-4.97835	2.47438	1.45236
H	-6.24693	2.03015	-1.57581
H	-3.32760	2.30719	3.08860
H	1.29921	-1.62027	3.81917
H	-1.83316	-5.73679	0.21283
H	-3.31910	-4.77588	0.08205
H	0.54795	-5.56159	0.88834
H	-4.12710	-0.18645	1.80784
H	-2.07906	3.57651	2.98957
H	1.92855	-2.66550	2.52063
H	-2.80179	-1.34773	1.53547
H	-1.69068	1.92447	2.50516
H	-1.83957	-4.25146	-0.76162
H	1.28614	-1.06681	2.13607
H	-4.11618	3.91914	-2.50042
H	-5.87663	-0.12899	0.26776
H	2.37319	-6.09143	-0.72140
H	-2.60599	0.34369	1.07743
H	-1.05016	5.80933	0.77980

H	-6.87493	-0.73596	-1.92956
H	1.19501	2.45570	3.87783
H	0.50270	1.04931	3.06313
H	1.51191	0.82014	4.51243
H	4.87243	-2.84081	-0.53474
H	-1.98672	4.59481	-3.12490
H	1.21309	6.43860	1.63700
H	4.03630	-1.65517	0.47076
H	3.37866	-4.24449	-2.07344
H	-0.96119	5.27274	-1.83236
H	-5.45144	-1.79325	-3.68134
H	-2.17669	-3.20192	-3.09769
H	-0.68335	3.62496	-2.39653
H	5.62626	-1.25875	-0.21613
H	-3.42355	-2.85142	-4.33298
H	2.91519	4.63652	1.96583
H	3.61216	-0.08311	4.03454
H	0.11176	-1.81397	-2.99282
H	1.03349	-2.70938	-4.19411
H	-2.11886	-1.69039	-4.00352
H	5.59713	0.21232	-2.01126
H	0.46699	-1.06510	-4.56970
H	3.31316	2.50222	-1.22910
H	3.86850	3.90773	-0.31307
H	5.82726	-1.49228	2.51737
H	6.15060	-0.42643	3.89371
H	2.34292	0.31381	-4.81650
H	5.05044	2.71620	-0.91737
H	5.89162	1.20027	0.62660
H	6.96327	-0.14183	2.33492
H	5.78344	1.44533	-4.23466
H	4.48799	2.51558	-3.67605
H	4.31927	1.66800	-5.22559
N	-1.76519	-1.72914	-0.98665
N	0.45166	-1.13144	-0.38801
N	0.10696	1.35173	0.38594
P	-0.84730	0.99910	-1.11966
P	1.23506	0.45937	-0.69018

4 References

- [1] H. Beer, J. Bresien, D. Michalik, A. Schulz, A. Villinger, *Dalton Trans.* **2020**, 49, 13986–13992.
- [2] U. Megerle, I. Pugliesi, C. Schriever, C. F. Sailer, E. Riedle, *Appl. Phys. B* **2009**, 96, 215–231.
- [3] C. V. Shank, E. P. Ippen, *Chem. Phys. Lett.* **1977**, 46, 129.
- [4] *Gaussian 09, Revision E.01*, M. J. Frisch, G. W. Trucks, H. B. Schlegel, G. E. Scuseria, M. A. Robb, J. R. Cheeseman, G. Scalmani, V. Barone, B. Mennucci, G. A. Petersson, H. Nakatsuji, M. Caricato, X. Li, H. P. Hratchian, A. F. Izmaylov, J. Bloino, G. Zheng, J. L. Sonnenberg, M. Hada, M. Ehara, K. Toyota, R. Fukuda, J. Hasegawa, M. Ishida, T. Nakajima, Y. Honda, O. Kitao, H. Nakai, T. Vreven, J. A. Montgomery Jr., J. E. Peralta, F. Ogliaro, M. Bearpark, J. J. Heyd, E. Brothers, K. N. Kudin, V. N. Staroverov, T. Keith, R. Kobayashi, J. Normand, K. Raghavachari, A. Rendell, J. C. Burant, S. S. Iyengar, J. Tomasi, M. Cossi, N. Rega, J. M. Millam, M. Klene, J. E. Knox, J. B. Cross, V. Bakken, C. Adamo, J. Jaramillo, R. Gomperts, R. E. Stratmann, O. Yazyev, A. J. Austin, R. Cammi, C. Pomelli, J. W. Ochterski, R. L. Martin, K. Morokuma, V. G. Zakrzewski, G. A. Voth, P. Salvador, J. J. Dannenberg, S. Dapprich, A. D. Daniels, O. Farkas, J. B. Foresman, J. V. Ortiz, J. Cioslowski, D. J. Fox, Gaussian, Inc., Wallingford CT, **2013**.
- [5] F. Neese, *WIREs Comput. Mol. Sci.* **2018**, 8, e1327.
- [6] J. P. Perdew, K. Burke, M. Ernzerhof, *Phys. Rev. Lett.* **1996**, 77, 3865–3868.
- [7] J. P. Perdew, K. Burke, M. Ernzerhof, *Phys. Rev. Lett.* **1997**, 78, 1396–1396.
- [8] C. Adamo, V. Barone, *J. Chem. Phys.* **1999**, 110, 6158–6170.
- [9] S. Grimme, J. Antony, S. Ehrlich, H. Krieg, *J. Chem. Phys.* **2010**, 132, 154104.
- [10] S. Grimme, S. Ehrlich, L. Goerigk, *J. Comput. Chem.* **2011**, 32, 1456–1465.
- [11] F. Weigend, R. Ahlrichs, *Phys. Chem. Chem. Phys.* **2005**, 7, 3297–305.
- [12] F. Weigend, *Phys. Chem. Chem. Phys.* **2006**, 8, 1057.
- [13] D. Hegarty, M. A. Robb, *Mol. Phys.* **1979**, 38, 1795–1812.
- [14] R. H. A. Eade, M. A. Robb, *Chem. Phys. Lett.* **1981**, 83, 362–368.
- [15] H. B. Schlegel, M. A. Robb, *Chem. Phys. Lett.* **1982**, 93, 43–46.
- [16] F. Bernardi, A. Bottoni, J. J. W. McDouall, M. A. Robb, H. B. Schlegel, *Faraday Symp. Chem. Soc.* **1984**, 19, 137.
- [17] P. E. M. Siegbahn, *Chem. Phys. Lett.* **1984**, 109, 417–423.
- [18] M. A. Robb, U. Niazi, in *Reports in Molecular Theory, Vol. 1* (Eds.: H. Weinstein, G.

- Náray-Szabó), CRC Press, Boca Raton, FL, **1990**, pp. 23–55.
- [19] M. J. Frisch, I. N. Ragazos, M. A. Robb, H. B. Schlegel, *Chem. Phys. Lett.* **1992**, *189*, 524–528.
- [20] N. Yamamoto, T. Vreven, M. A. Robb, M. J. Frisch, H. B. Schlegel, *Chem. Phys. Lett.* **1996**, *250*, 373–378.
- [21] M. Klene, M. A. Robb, M. J. Frisch, P. Celani, *J. Chem. Phys.* **2000**, *113*, 5653–5665.
- [22] C. Angeli, R. Cimiraglia, J.-P. Malrieu, *Chem. Phys. Lett.* **2001**, *350*, 297–305.
- [23] C. Angeli, R. Cimiraglia, S. Evangelisti, T. Leininger, J.-P. Malrieu, *J. Chem. Phys.* **2001**, *114*, 10252–10264.
- [24] C. Angeli, R. Cimiraglia, J.-P. Malrieu, *J. Chem. Phys.* **2002**, *117*, 9138–9153.
- [25] S. R. Langhoff, E. R. Davidson, *Int. J. Quantum Chem.* **1974**, *8*, 61–72.
- [26] L. Meissner, *Chem. Phys. Lett.* **1988**, *146*, 204–210.
- [27] J. Bresien, T. Kröger-Badge, S. Lochbrunner, D. Michalik, H. Müller, A. Schulz, E. Zander, *Chem. Sci.* **2019**, *10*, 3486–3493.
- [28] K. Ishida, K. Morokuma, A. Komornicki, *J. Chem. Phys.* **1977**, *66*, 2153–2156.
- [29] K. Fukui, *Acc. Chem. Res.* **1981**, *14*, 363–368.
- [30] R. Bauernschmitt, R. Ahlrichs, *Chem. Phys. Lett.* **1996**, *256*, 454–464.
- [31] M. E. Casida, C. Jamorski, K. C. Casida, D. R. Salahub, *J. Chem. Phys.* **1998**, *108*, 4439–4449.
- [32] R. E. Stratmann, G. E. Scuseria, M. J. Frisch, *J. Chem. Phys.* **1998**, *109*, 8218–8224.
- [33] G. J. Atchity, S. S. Xantheas, K. Ruedenberg, *J. Chem. Phys.* **1991**, *95*, 1862–1876.
- [34] M. Boggio-Pasqua, M. J. Bearpark, P. A. Hunt, M. A. Robb, *J. Am. Chem. Soc.* **2002**, *124*, 1456–1470.
- [35] M. A. Robb, in *Advanced Series in Physical Chemistry, Vol. 17: Conical Intersections: Theory, Computation and Experiment* (Eds.: W. Domcke, D.R. Yarkony, H. Köppel), World Scientific Publishing, Singapore, **2011**, pp. 3–50.